Chapter 5

Flow analysis of a two-layered micropolar fluid in a catheterized oesophageal tube under the influence of a dilating amplitude: Application to pre-diagnosis of oesophageal motility disorder

5.1 Introduction

Swallowing disorders are more common and frequently reported nowadays. According to Panebianco et al. (2020), these affect around 400000 - 800000 people annually worldwide, the reasons being random eating, sleeping just after having a meal, obesity, etc. The consequences create swallowing disorders in the human oesophagus,

The content of this chapter is published in Physica Scripta 99(08) (2024) 085020. DOI: doi.org/10.1088/1402-4896/ad5e03

leading to life-threatening conditions for the patients, such as Barrets' oesophagus, in which the inner lining of the oesophageal layer gets inflammation. These may culminate in the accumulation of cancerous cells (Sasegbon and Hamdy (2017)). In some cases, the motility of either contraction or relaxation of the oesophageal circular and longitudinal muscles gets disturbed. This happens when a patient suffers from Achalasia. There are also some cases of sliding hiatus hernia, in which the upper part of the stomach protrudes through the hiatus, bulging near the distal part of the oesophagus.

The first advice from the doctor to the patients suffering from such disorders is to go for pre-diagnosis and surgery if required. Pre-diagnosis is performed by inserting a thin and flexible tube, called a catheter, through the mouth and sometimes through the nose, which is termed as a Nasogastric tube, into the oesophagus (Kahrilas et al. (1995), Kahrilas et al. (2008)). Various types of tubes are available that can be used as per the human body's requirement, such as a Foley catheter, which is used for a long duration for kidney patients who cannot urinate by themselves.

Insertion of a catheter leads to several complications. Hence, several researchers carried out intense investigations. Among them, Kanai et al. (1970) and Roos and Lykoudis (1971) analyzed the problem of peristaltic pumping of ureteral flow with the inserted catheter. They theoretically formulated the changes in blood pressure when a catheter is inserted into an artery. Apart from many related results, they also found that blood pressure increases immensely at the distal end when a catheter is inserted. Their experimental validations, however, were not in good agreement, for which they cited various reasons.

Srivastava and Srivastava (1983) studied entrance effects of pulsatile blood flow with a two-phase model, and then Back (1994) evaluated time mean flow when dealing with the catheter in the coronary artery. Several studies have been conducted on inserting the catheter into an artery with the blood flow systems.

Back et al. (1996) delved into the effects of catheter insertion on flow rate within stenosed arteries, both pre- and post-angioplasty. They observed an inverse relationship between flow rate and catheter thickness. El Misiery et al. (2002a) explored the impact of inserted endoscopes and Carreau fluid on peristaltic pumping under zero Reynolds number and infinitely long wavelength conditions. They found

maximum pressure rise at zero flow rate across different radius ratios, power-law indices, and Weissenberg numbers.

Srivastava (2007) proposed a two-fluid model comprising a core suspension of erythrocytes in plasma and a peripheral layer of cell-free plasma to represent blood flow in small-diameter tubes. Quantitative analysis suggested suitability for hematocrit levels up to 40 % and vessel diameters up to 70 micrometers.

Hayat et al. (2006) investigated the peristaltic flow of a Jeffrey fluid between concentric tubes, focusing on endoscope effects. They noted an increased axial pressure gradient with higher friction forces and a non-monotonic relationship with wave amplitude.

Similarly, Hayat et al. (2008) examined endoscope influence on the peristaltic flow of a Jeffrey fluid through tubes, finding that frictional forces exhibited an opposite trend to pressure rise, with smaller forces on the inner tube than the outer one.

Srivastava and Rastogi (2010) explored blood flow through a narrow catheterised artery with non-symmetrical stenosis. They concluded that increasing catheter size led to increased flow resistance and decreased shear stress at the stenosis throat, reaching an asymptotic value of around half the artery size.

In addition to Computed Tomography (CT) scan and Barium oesophagram, the upper endoscopy (a method that involves catheterisation with video fluoroscopy) may be tackled to get a helpful result of diagnosis in a patient who suffers from swallowing disorders (Dziewas et al. (2021), Abu-Ghanem et al. (2022)).

Recently, Zidan et al. (2021) investigated to evaluate the entropy generation occurring within a catheterised stenosed artery. The analysis conducted by the researchers revealed that an enhancement in the stenosis height resulted in a heightened intensity of the shear stress profile at the arterial wall.

Khanduri and Sharma (2023) conducted a study to analyze the impact of nanoparticle shape, explicitly focusing on hybrid nano-particles on blood circulation within a compromised artery. The affected artery displayed stenosis along its arterial walls and thrombosis at the central region of the catheter.

The liquid or the medicines, such as antibiotics in a solution, fed through an orogastric or nasogastric tube to patients may be micropolar Williams (2008). By definition, it is a non-Newtonian fluid in which body couple effects entail the interactions between translational and rotational motions, giving rise to the coupling of stress and couple stresses and the coupling of velocity and micro-rotation. We are interested in the effects of various parameters of the micropolar fluid with a catheterised oesophageal tube, especially in the presence of micropolar parameter and coupling number.

Mekheimer and Kot (2008b) studied a micropolar model for axisymmetric blood flow in a tapered artery with modest stenosis but no axial symmetry. They talked about how a subclass of these micro fluids called micropolar fluids has fluid microelements that are thought to be stiff. In a vertical annulus, a micropolar fluid flows peristaltically, and Nadeem et al. (2010) examined the impact of heat transmission on this process.

Micropolar fluid has vast applications in physiology, engineering, and industry, such as urine transport from the kidney to the bladder swallowing through the oesophagus, chyme motion in the gastrointestinal tract, vasomotion of small blood vessels, and movement of spermatozoa in the human reproductive tract. This is the reason for much research on this fluid motion.

Recently, Abdelmalek et al. (2021) delved into the bioconvection of nanoparticles in the flow of a generalized micropolar fluid towards an accelerated stretched surface. They found that the micro-rotation velocity decreases as the buoyancy ratio constraint increases. Furthermore, they concluded that the motile organism profile decreases with an increase in the temperature difference parameter and the Peclet number.

In a separate study, Song et al. (2021) investigated the characteristics of Arrhenius activation energy and nonlinear thermal radiation in bio-convective Brinkman-type micropolar nanofluid flow. They observed an increasing change in velocity with the angular micropolar parameter and mixed convection constant. Additionally, they concluded that a larger bioconvection Lewis number and Peclet number decrease the concentration of microorganisms.

Usman et al. (2021) aimed to develop a thermal flow model for a generalized micropolar nanofluid with bioconvection, activation energy, and nonlinear thermal radiation applications. They found that the presence of activation energy is more effective in enhancing nanofluid concentration.

The fluid in the oesophagus has a different viscosity near the wall than it does in the duct's middle. In these circumstances, fluid transport processes in these organs cannot be explained by peristaltic analysis of fluid in tubes with a single layer of constant viscosity. These physiological considerations necessitate using a two-fluid model to study biofluid flow in biological systems.

A few researchers have studied the two-layered model of physiological fluid. When the tube's geometry is non-uniform, Srivastava and Srivastava (1982) looked at the peristaltic transport of the fluid. With applications to blood flow, Chaturani and Biswas (1983) investigated the three-layered Couette flow of polar fluid with non-zero particle spin boundary conditions at the interfaces. Pandey et al. (2015) investigated the mobility properties of the highly viscous multilayered intestinal fluid. When two immiscible viscous incompressible fluids move peristaltically in a circular tube.

In view of this, a two-phase flow with an inserted catheter surrounded by a micropolar fluid in the core region wrapped within an immiscible Newtonian fluid in the peripheral layer of the human oesophagus is planned to investigate. This mathematical model is expected to provide sound insights, particularly to clinicians, about the pre-diagnosis of swallowing disorders. Besides, answers sought to the following queries precisely reflect the objective of the article:

(i) What will be the impact of catheterisation when the core within the oesophagus is a micropolar fluid?

(ii) How does the presence of a micropolar parameter in the core affect the pressure distribution?

(iii) How is the pressure affected by the coupling number in the presence of an introduced catheter?

(iv) Does the broadening of the thickness of a catheter alter the pressure with the micropolar parameter and coupling number?

(v) What is the impact of catheterisation on Impedence?

(vi) Will it enhance the pressure if a micropolar fluid replaces the Newtonian fluid?

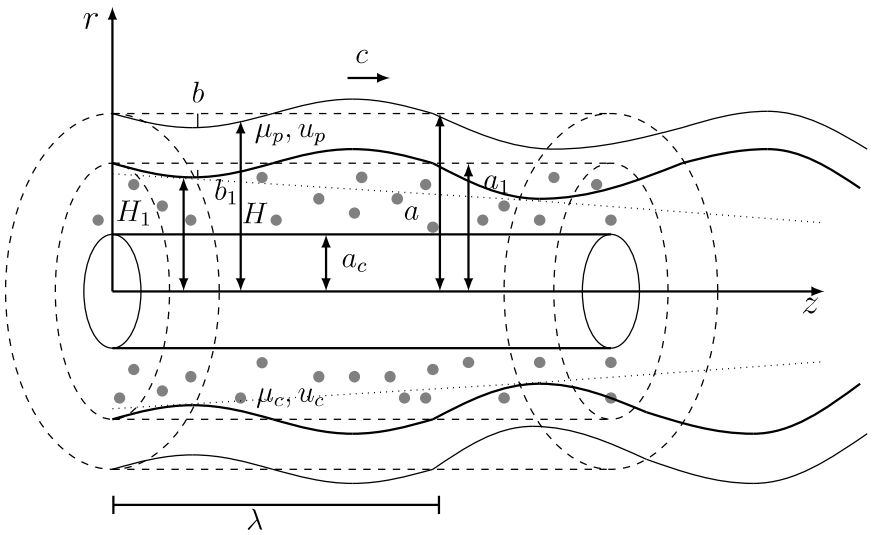

Figure 5.1: The schematic diagram illustrates three concentric circular cylindrical layers with radii in the order a, a_1, and a_c. The innermost layer is a rigid tube called a catheter, while the intermediate and outermost layers are micro-polar and Newtonian fluids of viscosities μ_p and μ_c, respectively. The distance from the central axis to the outermost boundary is H, and that to the interface between the Newtonian and the Micropolar fluids is H_1. A peristaltic wave of dilating wave amplitude travels down the outer layer at a speed c. The radial and the axial fluid velocities in the outer and the intermediate layers are respectively (w_1, v_p) and (w_r, w_z), in the r and z directions, respectively.

5.2 Mathematical formulation

Let us consider the peristaltic transport of a micropolar fluid surrounded co-axially by Newtonian fluid in an axisymmetric tube of radius a where a catheter of radius a_c is introduced (figure 5.1). Choosing the cylindrical polar coordinate system (Z, θ, R), the wall deformation due to the propagation of peristaltic waves is given by

$$H(Z,t) = a - be^{kZ}\cos^2\frac{\pi}{\lambda}(Z - ct), \tag{5.1}$$

where a, b, λ, t, c, and k are the tube radius, wave amplitude, wavelength, time, wave speed, and dilating amplitude parameter, respectively.

The equation for the interface between the two layers is assumed to be

$$H_1(Z,t) = a_1 - b_1 e^{kZ} \cos^2 \frac{\pi}{\lambda}(Z - ct), \tag{5.2}$$

where a_1 and b_1 are the radius of the core layer and wave amplitude, respectively.

The governing equation for the peripheral layer ($H_1 \leq R \leq H$) is given by Brasseur et al. (1987)

$$\rho_p\Big(\frac{\partial w_1}{\partial t} + w_1\frac{\partial w_1}{\partial z} + v_p\frac{\partial w_1}{\partial r}\Big) = -\frac{\partial p}{\partial z} + \mu_p\nabla^2 w_1, \tag{5.3}$$

$$\rho_p\Big(\frac{\partial v_p}{\partial t} + w_1\frac{\partial v_p}{\partial z} + v_p\frac{\partial v_p}{\partial r}\Big) = -\frac{\partial p}{\partial r} + \mu_p(\nabla^2 - \frac{1}{r^2})v_p, \tag{5.4}$$

$$\frac{1}{r}\frac{\partial}{\partial r}(rv_p) + \frac{\partial}{\partial z}(w_1) = 0, \tag{5.5}$$

where (w_1, v_p) and μ_p are the (axial, radial) velocities in (Z, R)-direction and the viscosity of the Newtonian fluid in the peripheral region, respectively. The Laplacian operator is given by $\nabla^2 \equiv \frac{\partial^2}{\partial r^2} + \frac{1}{r}\frac{\partial}{\partial r} + \frac{\partial^2}{\partial z^2}$.

The equations governing the unsteady flow of an incompressible micropolar fluid ($a_c \leq R \leq H_1$) in the absence of body force and body couple as given by Eringen (1966) are

$$\rho_c\Big(\frac{\partial w_r}{\partial t}+w_r\frac{\partial w_r}{\partial r}+w_z\frac{\partial w_r}{\partial z}\Big) = -\frac{\partial p}{\partial r}+\Big(\frac{2\mu_c+K}{2}\Big)\Big(\frac{\partial^2 w_r}{\partial r^2}+\frac{1}{r}\frac{\partial w_r}{\partial r}+\frac{\partial^2 w_r}{\partial z^2}-\frac{w_r}{r^2}-K\frac{\partial G}{\partial z}\Big), \tag{5.6}$$

$$\rho_c\Big(\frac{\partial w_z}{\partial t} + w_r\frac{\partial w_z}{\partial r} + w_z\frac{\partial w_z}{\partial z}\Big) = -\frac{\partial p}{\partial z} + \Big(\frac{2\mu_c+K}{2}\Big)\Big(\frac{\partial^2 w_z}{\partial r^2} + \frac{1}{r}\frac{\partial w_z}{\partial r} + \frac{\partial^2 w_z}{\partial z^2}\Big) + K\Big(\frac{\partial G}{\partial r} + \frac{G}{r}\Big), \tag{5.7}$$

$$\rho_c j\Big(\frac{\partial G}{\partial t}+w_r\frac{\partial G}{\partial r}+w_z\frac{\partial G}{\partial z}\Big) = -2KG+\Big(\frac{\partial^2 G}{\partial r^2}+\frac{1}{r}\frac{\partial G}{\partial r}+\frac{\partial^2 G}{\partial z^2}-\frac{G}{r^2}\Big)+K\Big(\frac{\partial w_r}{\partial z}-\frac{\partial w_z}{\partial r}\Big), \tag{5.8}$$

$$\frac{\partial w_r}{\partial r} + \frac{\partial w_z}{\partial z} + \frac{w_r}{r} = 0, \tag{5.9}$$

where ρ_c, μ_c, p, t, w_r, w_z, G, j, K and γ are density, dynamic viscosity coefficient, pressure, time, component of velocity in r-direction, component of velocity in z-direction, non-vanishing component of the micro-rotation vector in the θ-direction, micro-inertia constant, coefficients of vortex viscosity and gyro-viscosity respectively. Note that in our case, $G = v_\theta$, w_θ, and $v_r = v_z = 0$.

The transformations are as follows
$z = Z - ct$; $r = R$; $u = U - 1$; $v = V$; $p = p$; $q = Q - 1 = q_1 + q_2$.

The non-dimensional quantities are
$h' = \frac{H}{a}$, $h'_1 = \frac{H_1}{a}$, $r' = \frac{r}{a}$, $z' = \frac{z}{\lambda}$, $w'_1 = \frac{w_1}{c}$, $p' = \frac{pa^2}{c\lambda\mu_c}$, $w'_r = \frac{\lambda w_r}{ac}$, $w'_z = \frac{w_z}{c}$, $v'_\theta = \frac{av_\theta}{c}$, $t' = \frac{ct}{\lambda}$, $j' = \frac{j}{a^2}$. Using the non-dimensional quantities, the above equations are reduced to
for the peripheral layer $(h_1 \leq r \leq h)$:

$$\delta Re\Big(\frac{\partial w_1}{\partial t} + w_1\frac{\partial w_1}{\partial z} + v_p\frac{\partial w_1}{\partial r}\Big) = -\frac{\partial p}{\partial z} + \mu\Big(\frac{1}{r}\frac{\partial}{\partial r}(r\frac{\partial w_1}{\partial r}) + \delta^2\frac{\partial^2 w_1}{\partial z^2}\Big), \tag{5.10}$$

$$\delta^3 Re\Big(\frac{\partial v_p}{\partial t} + w_1\frac{\partial v_p}{\partial z} + v_p\frac{\partial v_p}{\partial r}\Big) = -\frac{\partial p}{\partial r} + \mu\Big(\delta^2\frac{1}{r}\frac{\partial}{\partial r}(r\frac{\partial v_p}{\partial r}) + \delta^4\frac{\partial^2 v_p}{\partial z^2} - \delta^2\frac{v_p}{r^2}\Big), \tag{5.11}$$

$$\frac{1}{r}\frac{\partial}{\partial r}(rv_p) + \frac{\partial w_1}{\partial z} = 0, \tag{5.12}$$

and for the core layer $(\epsilon \leq r \leq h_1)$:

$$Re\delta^3\Big(w_r\frac{\partial w_r}{\partial r} + w_z\frac{\partial w_r}{\partial z}\Big) = -\frac{\partial p}{\partial r} + \frac{\delta^2}{1-N}\Big(\frac{\partial^2 w_r}{\partial r^2} + \frac{1}{r}\frac{\partial w_r}{\partial r} + \delta^2\frac{\partial^2 w_r}{\partial z^2} - \frac{w_r}{r^2} - N\frac{\partial v_\theta}{\partial z}\Big), \tag{5.13}$$

$$Re\delta\Big(w_r\frac{\partial w_z}{\partial r} + w_z\frac{\partial w_z}{\partial z}\Big) = -\frac{\partial p}{\partial z} + \frac{1}{N-1}\Big(\frac{N}{r}\frac{\partial(rv_\theta)}{\partial r} + \frac{\partial^2 w_z}{\partial r^2} + \frac{1}{r}\frac{\partial w_z}{\partial r} + \delta^2\frac{\partial^2 w_z}{\partial z^2}\Big), \tag{5.14}$$

$$\begin{aligned}\frac{Re\delta j(1-N)}{N}\Big(w_r\frac{\partial v_\theta}{\partial r} + w_z\frac{\partial v_\theta}{\partial z}\Big) = &-2v_\theta + \frac{2-N}{m^2}\Big(\Big(\frac{1}{r}\frac{\partial(rv_\theta)}{\partial r}\Big) + \frac{\partial^2 v_\theta}{\partial z^2}\Big)\\ &+ \Big(\delta^2\frac{\partial w_r}{\partial z} - \frac{\partial w_z}{\partial r}\Big),\end{aligned} \tag{5.15}$$

$$\frac{\partial w_r}{\partial r} + \frac{\partial w_z}{\partial z} + \frac{w_r}{r} = 0, \tag{5.16}$$

where $N = \frac{K}{K+\mu_c}, (0 < N < 1)$, $m^2 = \frac{K(2\mu_c+K)a^2}{\gamma(K+\mu_c)}$. Here, N and m symbolize the coupling number and micropolar parameter, respectively.

Under the assumptions of long wavelength and low Reynolds number approximations, i.e., for wave number $\delta(=\frac{a}{\lambda}) << 1$ and Reynolds number $Re(=\frac{\rho a c}{\mu_c}) \to 0$, the above equations (5.10) to (5.16) reduce to

$$\frac{\partial p}{\partial z} = \frac{1}{r}\frac{\partial}{\partial r}\Big(r\mu\frac{\partial}{\partial r}\Big)w_1, \tag{5.17}$$

$$\frac{\partial p}{\partial r} = 0, \tag{5.18}$$

$$\frac{N}{r}\frac{\partial(rv_\theta)}{\partial r} + \frac{\partial^2 w_z}{\partial r^2} + \frac{1}{r}\frac{\partial w_z}{\partial r} = (1-N)\frac{\partial p}{\partial z}, \tag{5.19}$$

$$2v_\theta + \frac{\partial w_z}{\partial r} - \frac{2-N}{m^2}\frac{\partial}{\partial r}\Big(\frac{1}{r}\frac{\partial}{\partial r}(rv_\theta)\Big) = 0. \tag{5.20}$$

The non-dimensional boundary conditions are as follows:

$$w_1 = -1 \quad at \quad r = h, \tag{5.21}$$

$$w_z = -1, v_\theta = 0, \quad at \quad r = \epsilon, \tag{5.22}$$

$$\frac{\partial w_z}{\partial r} = 0, \quad at \quad r = \frac{\alpha-\epsilon}{2}, \tag{5.23}$$

$$w_1 = w_z, v_\theta = 0, \quad at \quad r = h_1. \tag{5.24}$$

The above boundary conditions are the typical no-slip conditions on the tube as well as the catheter's wall, and the velocity continuity at the contact (i.e., interface) are specified in Equations (5.21) to (5.24). Upon using the Equations (5.19) and (5.20), we write

$$\frac{\partial^2 w_z}{\partial r^2} + \frac{1}{r}\Big(\frac{\partial w_z}{\partial r} + Nv_\theta\Big) + N\frac{\partial v_\theta}{\partial r} = (1-N)\frac{dp}{dz}, \tag{5.25}$$

$$\frac{\partial^2 v_\theta}{\partial r^2} + \frac{1}{r}\frac{\partial v_\theta}{\partial r} - \Big(\frac{2m^2}{2-N} + \frac{1}{r^2}\Big)v_\theta = \frac{m^2}{2-N}\frac{\partial w_z}{\partial r}. \tag{5.26}$$

5.3 Analysis

Applying the Homotopy Perturbation Method, Equations (5.25) and (5.26), are written as

$$\frac{\partial^2 w_z}{\partial r^2} = s\Big[(1-N)\frac{dp}{dz} - \frac{1}{r}\Big(\frac{\partial w_z}{\partial r} + N v_\theta\Big) - N\frac{\partial v_\theta}{\partial r}\Big], \tag{5.27}$$

$$\frac{\partial^2 v_\theta}{\partial r^2} = s\Big[\frac{m^2}{2-N}\frac{\partial w_z}{\partial r} - \frac{1}{r}\frac{\partial v_\theta}{\partial r} + \Big(\frac{2m^2}{2-N} + \frac{1}{r^2}\Big)v_\theta\Big]. \tag{5.28}$$

We express w_z and v_θ in a series in terms of for $s(0 < s \leq 1)$ as

$$w_z = w_{z_0} + s w_{z_1} + s^2 w_{z_2} + s^3 w_{z_3} + o(s^4), \tag{5.29}$$

$$v_\theta = v_{\theta_0} + s v_{\theta_1} + s^2 v_{\theta_2} + s^3 v_{\theta_3} + o(s^4). \tag{5.30}$$

Using (5.29) and (5.30) in Equation (5.27) as well as in (5.28), we get

$$\begin{aligned}\frac{\partial^2}{\partial r^2}(w_{z_0} + s w_{z_1} + s^2 w_{z_2} + s^3 w_{z_3}) = {} & s\Big[(1-N)\frac{dp}{dz} - \frac{1}{r}\Big(\frac{\partial w_{z_0}}{\partial r} + N v_{\theta_0}\Big) - N\frac{\partial v_{\theta_0}}{\partial r}\Big] \\ & + s^2\Big[-\frac{1}{r}\Big(\frac{\partial w_{z_1}}{\partial r} + N v_{\theta_1}\Big) - N\frac{\partial v_{\theta_1}}{\partial r}\Big] \\ & + s^3\Big[-\frac{1}{r}\Big(\frac{\partial w_{z_2}}{\partial r} + N v_{\theta_2}\Big) - N\frac{\partial v_{\theta_2}}{\partial r}\Big] + o(s^4),\end{aligned} \tag{5.31}$$

$$\begin{aligned}\frac{\partial^2}{\partial r^2}(v_{\theta_0} + s v_{\theta_1} + s^2 v_{\theta_2} + s^3 v_{\theta_3}) = {} & s\Big[\frac{m^2}{2-N}\frac{\partial w_{z_0}}{\partial r} - \frac{1}{r}\frac{\partial v_{\theta_0}}{\partial r} + \Big(\frac{2m^2}{2-N} + \frac{1}{r^2}\Big)v_{\theta_0}\Big] \\ & + s^2\Big[\frac{m^2}{2-N}\frac{\partial w_{z_1}}{\partial r} - \frac{1}{r}\frac{\partial v_{\theta_1}}{\partial r} + \Big(\frac{2m^2}{2-N} + \frac{1}{r^2}\Big)v_{\theta_1}\Big] \\ & + s^3\Big[\frac{m^2}{2-N}\frac{\partial w_{z_2}}{\partial r} - \frac{1}{r}\frac{\partial v_{\theta_2}}{\partial r} + \Big(\frac{2m^2}{2-N} + \frac{1}{r^2}\Big)v_{\theta_2}\Big] + o(s^4).\end{aligned} \tag{5.32}$$

On integrating Equation (5.17) and then using the boundary condition (5.21), we obtain

$$w_1 = \frac{1}{4\mu}\frac{dp}{dz}(r^2 - h^2) + c_1 \log\Big(\frac{r}{h}\Big). \tag{5.33}$$

5.3.1 Solution for the zeroth order

Comparing the coefficient of s^0 on both sides of Equations (5.31) and (5.32), we get

$$\frac{\partial^2}{\partial r^2}(w_{z_0}) = 0, \tag{5.34}$$

$$\frac{\partial^2}{\partial r^2}(v_{\theta_0}) = 0. \tag{5.35}$$

An integration of (5.34) and (5.35), with respect to r, by using the conditions (5.22), (5.23) and (5.24), we get

$$w_{z_0} = -1, \tag{5.36}$$

$$v_{\theta_0} = 0. \tag{5.37}$$

5.3.2 Solution for the first order

Comparing the coefficient of s^1 on both sides of Equations (5.31) and (5.32), we have

$$\frac{\partial^2}{\partial r^2}(w_{z_1}) = (1-N)\frac{dp}{dz} - \frac{1}{r}\Big(\frac{\partial w_{z_0}}{\partial r} + N v_{\theta_0}\Big) - N\frac{\partial v_{\theta_0}}{\partial r}, \tag{5.38}$$

$$\frac{\partial^2}{\partial r^2}(v_{\theta_1}) = \frac{m^2}{2-N}\frac{\partial w_{z_0}}{\partial r} - \frac{1}{r}\frac{\partial v_{\theta_0}}{\partial r} + \Big(\frac{2m^2}{2-N} + \frac{1}{r^2}\Big)v_{\theta_0}. \tag{5.39}$$

Solution for Equation (5.38) and (5.39) may be obtained using the boundary conditions (5.22), (5.23) and (5.24) as

$$w_{z_1} = (1-N)\frac{dp}{dz}\Big(\frac{r^2}{2} - \frac{(\alpha-\epsilon)}{2}r - \epsilon^2 + \frac{\alpha\epsilon}{2}\Big), \tag{5.40}$$

$$v_{\theta_1} = 0. \tag{5.41}$$

5.3.3 Solution for the second order

Comparing the coefficient of s^2 on both sides of Equations (5.31) and (5.32), we write

$$\frac{\partial^2}{\partial r^2}(w_{z_2}) = -\frac{1}{r}\Big(\frac{\partial w_{z_1}}{\partial r} + N v_{\theta_1}\Big) - N\frac{\partial v_{\theta_1}}{\partial r}, \tag{5.42}$$

$$\frac{\partial^2}{\partial r^2}(v_{\theta_2}) = \frac{m^2}{2-N}\frac{\partial w_{z_1}}{\partial r} - \frac{1}{r}\frac{\partial v_{\theta_1}}{\partial r} + \Big(\frac{2m^2}{2-N} + \frac{1}{r^2}\Big)v_{\theta_1}. \tag{5.43}$$

Solutions of Equations (5.42) and (5.43) by integrating w.r.t. r, (5.40) and (5.41) under the boundary conditions (5.22), (5.23) and (5.24), may be given by

$$w_{z_2} = -\frac{1-N}{2}\frac{dp}{dz}\Big(\frac{r^2}{2} - (\alpha-\epsilon)(\log(r)-1)r + A_1(r-\epsilon) + A_2\Big), \tag{5.44}$$

where $A_1 = -\frac{\alpha-\epsilon}{2} + (\alpha-\epsilon)\log(\alpha-\epsilon)$, and $A_2 = -\frac{\epsilon^2}{2} + (\alpha-\epsilon)(\log(\epsilon)-1)\epsilon$.

$$v_{\theta_2} = -\frac{m^2(1-N)}{4(2-N)}\frac{dp}{dz}\Big(\frac{r^3}{3} - (\alpha-\epsilon)r^2 + rA_3 + A_4\Big), \tag{5.45}$$

where $A_3 = (\alpha-\epsilon)(h_1+\epsilon) - \frac{1}{3}(h_1^2+\epsilon^2+h_1\epsilon)$ and $A_4 = -(\alpha-\epsilon)\epsilon h_1 - \frac{1}{3}(\epsilon^2+h_1\epsilon)$.

5.3.4 Solution for the third order

Comparing the coefficient of s^2 on both side of equations (5.31) and (5.32), we have

$$\frac{\partial^2}{\partial r^2}(w_{z_3}) = -\frac{1}{r}\Big(\frac{\partial w_{z_2}}{\partial r} + Nv_{\theta_2}\Big) - N\frac{\partial v_{\theta_2}}{\partial r}, \tag{5.46}$$

$$\frac{\partial^2}{\partial r^2}(v_{\theta_3}) = \frac{m^2}{2-N}\frac{\partial w_{z_2}}{\partial r} - \frac{1}{r}\frac{\partial v_{\theta_2}}{\partial r} + \Big(\frac{2m^2}{2-N} + \frac{1}{r^2}\Big)v_{\theta_2}. \tag{5.47}$$

We write the solutions of integration of the equations (5.46) and (5.47) by using equations (5.44) and (5.45) with the boundary conditions (5.22), (5.23) and (5.24) as

$$\begin{aligned} w_{z_3} = \frac{m^2N(1-N)}{(2-N)}\frac{dp}{dz}\Big[&-\frac{r^4}{48} + (\alpha-\epsilon)\frac{r^3}{12} - \frac{r^2}{8}A_3 + \frac{2-N}{2Nm^2}\Big\{\frac{r^2}{2} - \frac{\alpha-\epsilon}{2}(r(\log(r))^2 \\ &- 6r\log(r) + 6r) + r(\log(r)-1)A_1\Big\} - \frac{r^4}{144} + \frac{\alpha-\epsilon}{24}r^3 + \frac{r^2}{2}A_3 + r(\log(r) \\ &- 1)\frac{A_4}{4} + rC_5 + C_6\Big], \end{aligned} \tag{5.48}$$

where $C_5 = -\Big(-\frac{(\alpha-\epsilon)^3}{48} - \frac{(\alpha-\epsilon)}{8}A_3 + \frac{2-N}{2Nm^2}\Big\{\frac{(\alpha-\epsilon)}{2}(1-(\log(\alpha-\epsilon)/2)^2 + 4\log((\alpha-\epsilon)/2)) + A_1\log((\alpha-\epsilon)/2)\Big\} + \frac{(\alpha-\epsilon)^3}{288} + \frac{(\alpha-\epsilon)}{2}A_3 + \frac{A_4}{4}\log((\alpha-\epsilon)/2)\Big)$ and $C_6 = -\frac{5}{48}\epsilon^4 + \frac{\alpha\epsilon^3}{12} - \frac{\epsilon^3}{8}A_3 + \frac{2-N}{2Nm^2}\Big\{\frac{\epsilon^2}{2} - \frac{(\alpha-\epsilon)}{2}(\epsilon(\log(\epsilon))^2 - 6\epsilon\log(\epsilon) + 6\epsilon) + A_1\epsilon(\log(\epsilon)-1)\Big\} - \frac{\epsilon^4}{144} +$

$\frac{(\alpha-\epsilon)}{24}\epsilon^3+\frac{\epsilon^2}{2}A_3+\frac{A_4}{4}\epsilon(\log(\epsilon)-1)$,

$$v_{\theta_3}=\frac{m^2(1-N)}{2-N}\frac{dp}{dz}\Big[(\frac{\alpha-\epsilon}{4})r^2(\log(r)-3/2)-\frac{r^3}{9}+(\frac{\alpha-\epsilon}{8})r^2-\frac{r^2}{4}A_1+\frac{3A_4}{2r^4}+\frac{2m^2}{2-N}\Big(\frac{r^5}{240}-\frac{r^4}{48}(\alpha-\epsilon)+\frac{r^3}{24}A_3+\frac{r^2}{8}A_4\Big)+rA_5+A_6\Big], \tag{5.49}$$

where $A_5=\frac{1}{(h_1-\epsilon)}\Big[(\frac{\alpha-\epsilon}{4})(\epsilon^2(\log(\epsilon)-3/2)-h_1^2(\log(h_1)-3/2))-\frac{\epsilon^3-h_1^3}{9}+(\frac{\alpha-\epsilon}{8})(\epsilon^2-h_1^2)-\frac{(\epsilon^2-h_1^2)}{4}A_1+\frac{3(h_1^4-\epsilon^4)A_4}{2\epsilon^4h_1^4}+\frac{2m^2}{2-N}\Big(\frac{(\epsilon^5-h_1^5)}{240}-\frac{(\epsilon^4-h_1^4)}{48}(\alpha-\epsilon)+\frac{(\epsilon^3-h_1^3)}{24}A_3+\frac{(\epsilon^2-h_1^2)}{8}A_4\Big)\Big]$, and

$A_6=\frac{1}{(\epsilon-h_1)}\Big[h_1\Big\{(\frac{\alpha-\epsilon}{4})\epsilon^2(\log(\epsilon)-3/2)-\frac{\epsilon^3}{9}+(\frac{\alpha-\epsilon}{8})\epsilon^2-\frac{\epsilon^2}{4}A_1+\frac{3A_4}{2\epsilon^4}+\frac{2m^2}{2-N}\Big(\frac{\epsilon^5}{240}-\frac{\epsilon^4}{48}(\alpha-\epsilon)+\frac{\epsilon^3}{24}A_3+\frac{\epsilon^2}{8}A_4\Big)\Big\}-\epsilon\Big\{(\frac{\alpha-\epsilon}{4})^2(\log(h_1)-3/2)-\frac{h_1^3}{9}+(\frac{\alpha-\epsilon}{8})h_1^2-\frac{h_1^2}{4}A_1+\frac{3A_4}{2h_1^4}+\frac{2m^2}{2-N}\Big(\frac{h_1^5}{240}-\frac{h_1^4}{48}(\alpha-\epsilon)+\frac{h_1^3}{24}A_3+\frac{h_1^2}{8}A_4\Big)\Big\}\Big]$.

Combining the equations (5.36), (5.40), (5.44) and (5.48), we write for $s\to 1$ as

$$w_z=-1+\frac{m^2N(1-N)}{2-N}\frac{dp}{dz}\Big[-\frac{r^4}{48}+(\frac{\alpha-\epsilon}{12})r^3-\frac{A_3}{8}r^2+\frac{2-N}{2Nm^2}\Big\{\frac{r^2}{2}-\frac{\alpha-\epsilon}{2}(r(\log(r))^2-6r\log(r)+6r)+r(\log(r)-1)A_1\Big\}-\frac{r^4}{144}+\frac{\alpha-\epsilon}{24}r^3+\frac{r^2}{2}A_3+r(\log(r)-1)\frac{A_4}{4}+rC_5+C_6+\frac{2-N}{Nm^2}\Big\{\frac{r^2}{4}-(\alpha-\epsilon)r+(r-\epsilon)A_1+(\frac{\alpha-\epsilon}{2})r\log(r)+\alpha\epsilon-\frac{\epsilon^2}{2}+A_2\Big\}\Big]. \tag{5.50}$$

If $\epsilon\to 0$, this case reduces to the study of without introduced catheter for two-layered flow by Shapiro et al. (1969), Srivastava and Srivastava (1983), Srivastava (2007) and (Hayat et al. (2006), Hayat et al. (2008)). In addition, if $k\to 0$ and $\alpha\to 1$, the above case reduces to uniform wave amplitude and single layer case, respectively. Since we have employed the Homotopy perturbation technique to get the analytical solutions, which has not been done in earlier studies, it is not possible that all our results will be reduced to the existing literature.

From the equations (5.37), (5.41), (5.45) and (5.49), on combining these equations we get

$$v_\theta = \frac{m^(1-N)}{2-N}\frac{dp}{dz}\Big[-\frac{r^3}{36}+(\frac{\alpha-\epsilon}{4})r^2(\log(r)-2)+(A_3+A_5)r-(\frac{r^2}{4})A_4+\frac{3A_4}{2r^4} + (A_4+A_6)+\frac{2m^2}{2-N}\Big(\frac{r^5}{240}-(\frac{\alpha-\epsilon}{48})r^4+\frac{A_3}{24}r^3+\frac{A_4}{8}r^2\Big)\Big]. \tag{5.51}$$

To get rid of the constant that is present in the equation (5.33), we use the equation (5.50) with the first term of the boundary condition (5.24), and then we write finally the peripheral layer velocity as

$$w_1 = \frac{m^2N(1-N)}{2-N}\frac{dp}{dz}\Bigg[A_7-\frac{(2-N)(h_1^2-h^2)}{4\mu m^2N(1-N)} + \frac{(2-N)(r^2-h^2)}{4\mu m^2N(1-N)}\frac{\log(h_1/h)}{\log(r/h)}\Bigg]\frac{\log(r/h)}{\log(h_1/h)}-\frac{\log(r/h)}{\log(h_1/h)}, \tag{5.52}$$

where $A_7 = -\frac{h_1^4}{48}+(\frac{\alpha-\epsilon}{12})h_1^3-\frac{A_3}{8}h_1^2+\frac{2-N}{2Nm^2}\Big\{\frac{h_1^2}{2}-\frac{\alpha-\epsilon}{2}(h_1(\log(h_1))^2-6h_1\log(h_1)+6h_1)+h_1(\log(h_1)-1)A_1\Big\}-\frac{h_1^4}{144}+\frac{\alpha-\epsilon}{24}h_1^3+\frac{h_1^2}{2}A_3+h_1(\log(h_1)-1)\frac{A_4}{4}+h_1C_5+C_6+\frac{2-N}{Nm^2}\Big\{\frac{h_1^2}{4}-(\alpha-\epsilon)h_1+(h_1-\epsilon)A_1+(\frac{\alpha-\epsilon}{2})h_1\log(h_1)+\alpha\epsilon-\frac{\epsilon^2}{2}+A_2$.
Now, using the computed value of core and peripheral layers velocity in the expressions (5.50) and (5.52), respectively, we write the volume flow rate in wave frame as

$$q = \int_\epsilon^{h_1} 2rw_z dr + \int_{h_1}^{h} 2rw_1 dr, \tag{5.53}$$

$$q = \xi + \frac{2m^2N(1-N)}{2-N}\frac{dp}{dz}(\eta), \tag{5.54}$$

where $\xi = 2\Big(\frac{h^2}{4\log(h_1/h)}-\frac{h^2(\log(h_1/h)-1/2)}{2\log(h_1/h)}-\frac{(h_1^2-\epsilon^2)}{2}\Big)$, and
$\eta = \Big[\Big\{A_7-\frac{(2-N)(h_1^2-h^2)}{4\mu m^2N(1-N)}+\frac{2(2-N)h}{3\mu m^2N(1-N)}\log(h_1/h)\Big\}\frac{(-h^2)}{4\log(h_1/h)}-\Big\{A_7-\frac{(2-N)(h_1^2-h^2)}{4\mu m^2N(1-N)} + \frac{(2-N)(h_1^2/3-h^2)}{2\mu h_1m^2N(1-N)}\frac{\log(h_1/h)}{(\log(h_1/h)-1/2)}\Big\}\frac{h_1^2(\log(h_1/h)-1/2)}{2\log(h_1/h)}-\frac{(h_1^6-\epsilon^6)}{288}-\frac{(\alpha-\epsilon)}{60}(h_1^5-\epsilon^5)-\frac{A_3}{32}(h_1^4-\epsilon^4)+\frac{2-N}{2Nm^2}\Big\{\frac{(h_1^6-\epsilon^6)}{8}-\frac{(\alpha-\epsilon)}{6}((h_1^3(\log(h_1))^2-\log(h_1)+1/3)-(\epsilon^3(\log(\epsilon))^2-\log(\epsilon)+1/3)-3h_1^2(\log(h_1)-1/2)+3\epsilon^2(\log(\epsilon)-1/2)+2(h_1^3-\epsilon^3))+A_1(\frac{h_1^3}{3}(\log(h_1)-4/3)-\frac{\epsilon^3}{3}(\log(\epsilon)-4/3))+\frac{(h_1^4-\epsilon^4)}{16}-\frac{(\alpha-\epsilon)}{3}(h_1^3-\epsilon^3)+A_1(\frac{h_1^3-\epsilon^3}{3}-\frac{\epsilon}{2}(h_1^2-\epsilon^2))+\frac{(\alpha-\epsilon)}{6}((h_1^3(\log(h_1))^2-\log(h_1)+1/3)-(\epsilon^3(\log(\epsilon))^2-\log(\epsilon)+1/3)+(\alpha\epsilon-\frac{\epsilon^2}{2})(\frac{h_1^2-\epsilon^2}{2})+\frac{A_2}{2}(h_1^2-\epsilon^2)\Big\}-\Big\{\frac{(h_1^6-\epsilon^6)}{864}+\frac{(\alpha-\epsilon)}{120}(h_1^2-$

$\epsilon^2)+\frac{A_3}{8}(h_1^4-\epsilon^4)+\frac{A_4}{8}(h_1^2(\log(h_1)-3/2)-\epsilon^2(\log(\epsilon)-3/2))+\frac{C_5}{3}(h_1^3-\epsilon^3)+\frac{C_6}{2}(h_1^2-\epsilon^2)\Big\}\Big]$.
Thus from (5.54), we write

$$\frac{dp}{dz}=\frac{(2-N)}{2m^2N(1-N)}\Big(\frac{q-\xi}{\eta}\Big). \tag{5.55}$$

The pressure is given by

$$\Delta p=\frac{(2-N)}{2m^2N(1-N)}\int_0^z\Big(\frac{q-\xi}{\eta}\Big)dz. \tag{5.56}$$

Following Shapiro et al. (1969), the time-averaged volume flow rate $\overline{Q}$ defined by $\overline{Q}=q+\int_0^1 h(z,t)dt$, h being the wall's surface as defined in equation (5.1) in the non-dimensional form, is

$$\overline{Q}=(q+1)+\frac{3}{8}\phi^2e^{2kz}-\phi e^{kz}, \tag{5.57}$$

from (5.56) and (5.57), we write as

$$\Delta p=\frac{(2-N)}{2m^2N(1-N)}\int_0^z\Big(\frac{\overline{Q}-1-\frac{3}{8}\phi^2e^{2kz}+\phi e^{kz}-\xi}{\eta}\Big)dz. \tag{5.58}$$

Take $I_1=\int_0^z\frac{1}{\eta}dz$, $I_2=\int_0^z\frac{e^{kz}}{\eta}dz$, $I_3=\int_0^z\frac{e^{2kz}}{\eta}dz$, and $I_4=\int_0^z\frac{\xi}{\eta}dz$,
we rewrite the above equation as

$$\Delta p=\frac{(2-N)}{2m^2N(1-N)}\Big((\overline{Q}-1)I_1+\phi I_2-\frac{3}{8}\phi^2I_3-I_4\Big). \tag{5.59}$$

The pressure that must be applied to achieve a zero-average flow rate which is written as

$$\Delta p_0=\frac{(2-N)}{2m^2N(1-N)}\Big(-I_1+\phi I_2-\frac{3}{8}\phi^2I_3-I_4\Big). \tag{5.60}$$

The time-averaged flux at zero pressure is given by

$$\overline{Q}_0=1-\phi\frac{I_2}{I_1}+\phi^2\frac{3I_3}{8I_1}+\frac{I_4}{I_1}. \tag{5.61}$$

Using the equations (5.59), (5.60) and (5.61), we write

$$\overline{Q} = \overline{Q}_0\Big(1 - \frac{\Delta p}{\Delta p_0}\Big). \tag{5.62}$$

The friction force $F_a(= f_a/\pi\lambda c\mu_p)$ at the tube wall across the axial length is now obtained as

$$F_a = \int_0^z h^2 \frac{dp}{dz} dz. \tag{5.63}$$

Therefore,

$$F_a = \frac{(2-N)}{2m^2N(1-N)}\Big((\overline{Q}-1)A_1 - \frac{3\phi^2}{8}A_2 + \phi A_3 - A_4\Big), \tag{5.64}$$

where $A_1 = \int_0^z \frac{h^2}{\eta} dz$, $A_2 = \int_0^z \frac{h^2 e^{2kz}}{\eta} dz$, $A_3 = \int_0^z \frac{h^2 e^{kz}}{\eta} dz$ and $A_4 = \int_0^z \frac{h^2 \xi}{\eta} dz$.
The friction force $F_c(= f_c/\pi\lambda c\mu_c)$ at the catheter wall across the axial length is now derived as

$$F_c = \int_0^z \epsilon^2 \frac{dp}{dz} dz. \tag{5.65}$$

Thus,

$$F_c = \frac{(2-N)\epsilon^2}{2m^2N(1-N)}\Big[(\overline{Q}-1)B_1 - \frac{3\phi^2}{8}B_2 + \phi B_3 - B_4\Big], \tag{5.66}$$

where $B_1 = \int_0^z \frac{1}{\eta} dz$, $B_2 = \int_0^z \frac{e^{2kz}}{\eta} dz$, $B_3 = \int_0^z \frac{e^{kz}}{\eta} dz$ and $B_4 = \int_0^z \frac{\xi}{\eta} dz$.
Using $\alpha = 1$, $\mu = 1$ for the no catheter case ($\epsilon \to 0$), the results of Shapiro et al. (1969) are recovered from the current study.

5.4 Results and Discussions

The code for the equations (5.50), (5.51), (5.58), and (5.66) for core layer velocity, peripheral layer velocity, pressure, and the frictional force due to the tube wall, respectively have been computed using MATLAB 2017Rb.

Various flow parameters are considered for the purpose of the study, and the practicality of these parametric values is their foundational aspect. These are all given in non-dimensional form, granting us the flexibility to select values within specific ranges. In determining these parameters, we adhered to the methodology

outlined by Brasseur et al. (1987) in their published work. For instance, the symbol α represents the ratio of peripheral layer thickness to the tube radius. As a result, α falls within the range of 0 to 1, where 0 signifies the absence of a peripheral layer, while 1 indicates the absence of a core layer. The figures illustrate that the practical range for α is typically below 0.4. However, it's important to note that our analysis is primarily qualitative. When examining the influence of viscosity on peripheral layers, we use a value of 0.4 solely for clarity. In certain instances, we choose 0.2 for the same reason. As for the symbol ϕ, which represents dimensionless wave amplitude, it can take values from 0 to 1. Based on anatomical measurements by Xia et al. (2009), the estimated dimensionless ϕ ranges from 0.47 to 0.8043, corresponding to a value of k equal to 0.134. For clarity, we assume that k is less than 0.1, which is a reasonable approximation. The value ϵ is assigned as 0.1, which is considered ideal. All detailed calculations are available in the appendix of Pandey et al. (2017) publication.

The pressure distribution along the considered oesophageal length is studied in figures 5.2(a-e). This study aims to get prior ideas before and after introducing a catheter into the oesophagus. The observation is that initially, the pressure is reduced to take the bolus inside through the upper oesophageal sphincter. Then, it spikes as the bolus and time pass through the action of circular and longitudinal muscles. The time constraints are taken from $t = 0$ to 1. Significantly, it is observed that the case without introducing a catheter, where the magnitude of the curves representing pressure distribution is relatively less midway to a bolus for micropolar fluid in comparison to that of Pandey et al. (2017) and Pandey and Pandey (2024d), who studied Newtonian fluid. It is further observed that the broadening of the catheter size ($\epsilon = 0.0 - 0.1$) increases the complications due to the increase in the pressure for a patient when they undergo catheterisation diagnosis. This agrees with the study of Muthu et al. (2008) and Srinivasacharya and Srikanth (2012) on artery catheterisation.

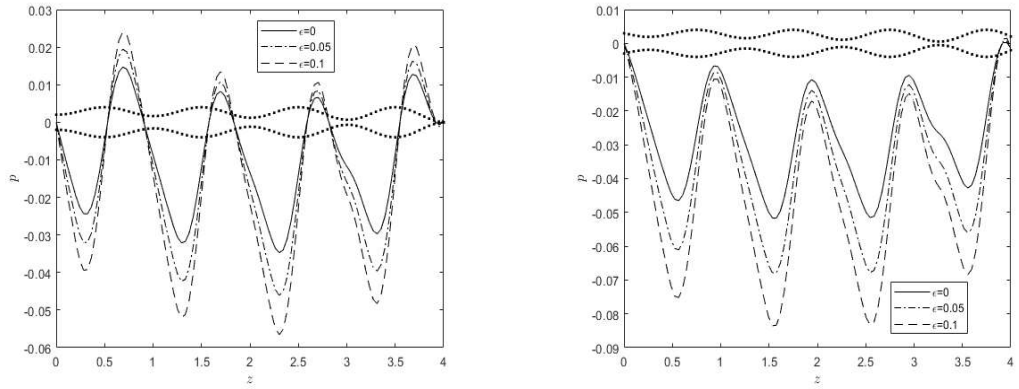

(a)

(b)

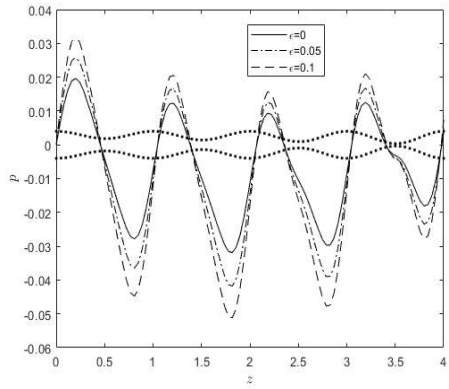

(c)

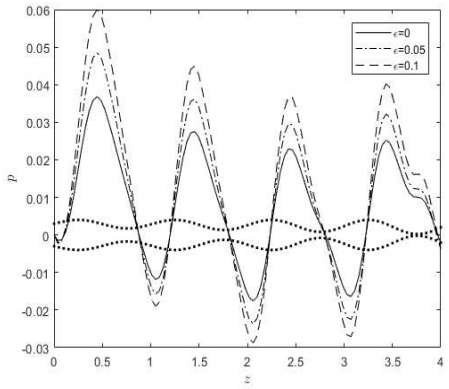

(d)

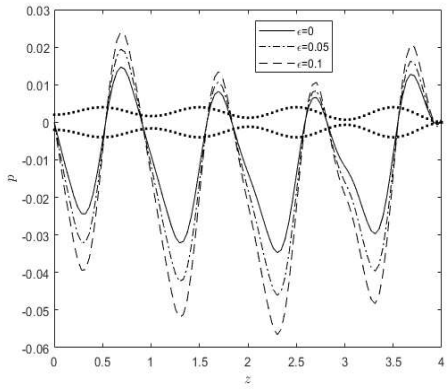

(e)

Figure 5.2: The plots show the pressure distribution along the oesophageal length for $\epsilon = 0.0 - 0.1$. Other parameters are being fixed as follows: $\phi = 0.49$, $\alpha = 0.4$, $\mu = 0.2$, $m = 5$, $N = 0.1$, $k = 0.07$, (a) $t = 0$, (b) $t = 0.25$, (c) $t = 0.5$, (d) $t = 0.75$, (e) $t = 1$.

In figures 5.3(a-e), the effect of dilating amplitude parameters on pressure distribution when the oesophageal tube is catheterised is discussed. The concept of dilating amplitude arose when Kahrilas et al. (1995) wrote in his article about the higher pressure requirement at the distal part of an oesophagus. It was further studied and verified experimentally by Xia et al. (2009) that pressure increases at the lower oesophageal sphincter to put a bolus completely into the stomach. Pandey et al. (2017) gave a mathematical view. In our study, we observe the large magnitude of the pressure distribution curves when increasing the dilating amplitude parameter (k) with the introduced catheter. Also, we can observe a constant propagation of waves when there is a case of no dilation (i.e., $k = 0$) and without introducing a catheter; this is aligned with the study of Brasseur et al. (1987). However, the effect of the dilating amplitude parameter is more on pressure distribution than in the study of Pandey and Pandey (2024d), who investigated Newtonian fluid with the introduced catheter.

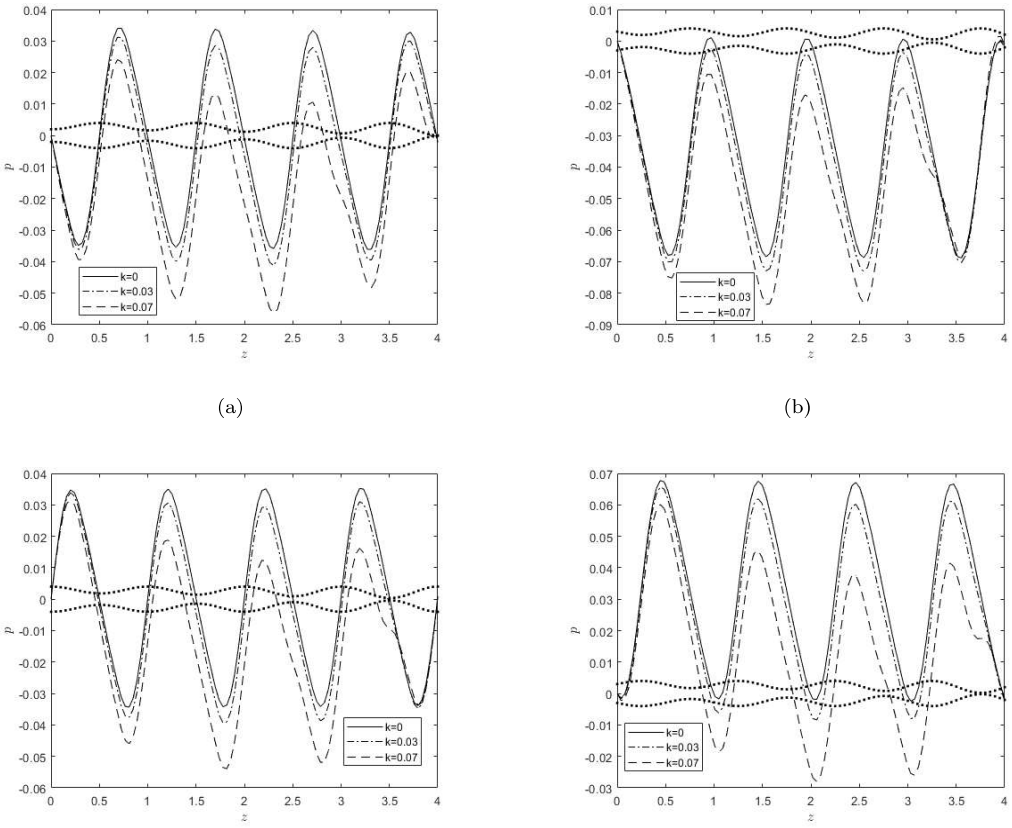

(a) (b)

(c) (d)

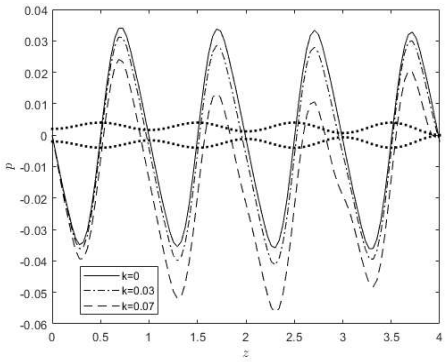

(e)

Figure 5.3: The plots show the pressure distribution along the catheterised oesophageal length for $k = 0.0 - 0.07$. Other parameters are being fixed as follows: $\phi = 0.49$, $\alpha = 0.4$, $\mu = 0.2$, $\epsilon = 0.1$, $m = 5$, $N = 0.1$, (a) $t = 0$, (b) $t = 0.25$, (c) $t = 0.5$, (d) $t = 0.75$, (e) $t = 1$.

In figures 5.4(a-e), upon varying the micropolar parameter (m) and keeping the other parameters, such as $\phi = 0.49$, $N = 0.1$, $k = 0.07$, $\alpha = 0.4$, $\mu = 0.2$, and $\epsilon = 0.2$ fixed the influence of the micropolar parameter affects the flow dynamics. It may be worth noting that when the micropolar parameter is dropped, this study reduces to the two-layered model incorporated by Pandey and Pandey (2024b) for the Newtonian fluid. Our comparative study with and without the introduced catheter has been done in this paper, given the alteration in the pressure distribution along the oesophageal length. During oesophageal catheterisation, the pressure exerted by the oesophageal walls is higher compared to no catheter case. No comparison to Newtonian fluids is possible since no value of m can result in Newtonian nature. We observe that the curve corresponding to $m = 5$, which represents the pressure distribution, decreases initially, and it is even higher for the same value compared to $m = 6$ and 7. The micropolar parameter is a significant determinant of the fall and increase of pressure over the entire length of the tube from $t = 0$ to 1 with the introduced catheter. We observed that as m rises, i.e., the gyro-viscosity decreases, the pressure falls over the whole length of the oesophageal tube. This means the micropolar parameter in the micropolar fluid helps diagnose swallowing disorder under catheterization when a patient needs to feed because, in the plots of the figure (5.2), we see that pressure increases with the introduced catheter.

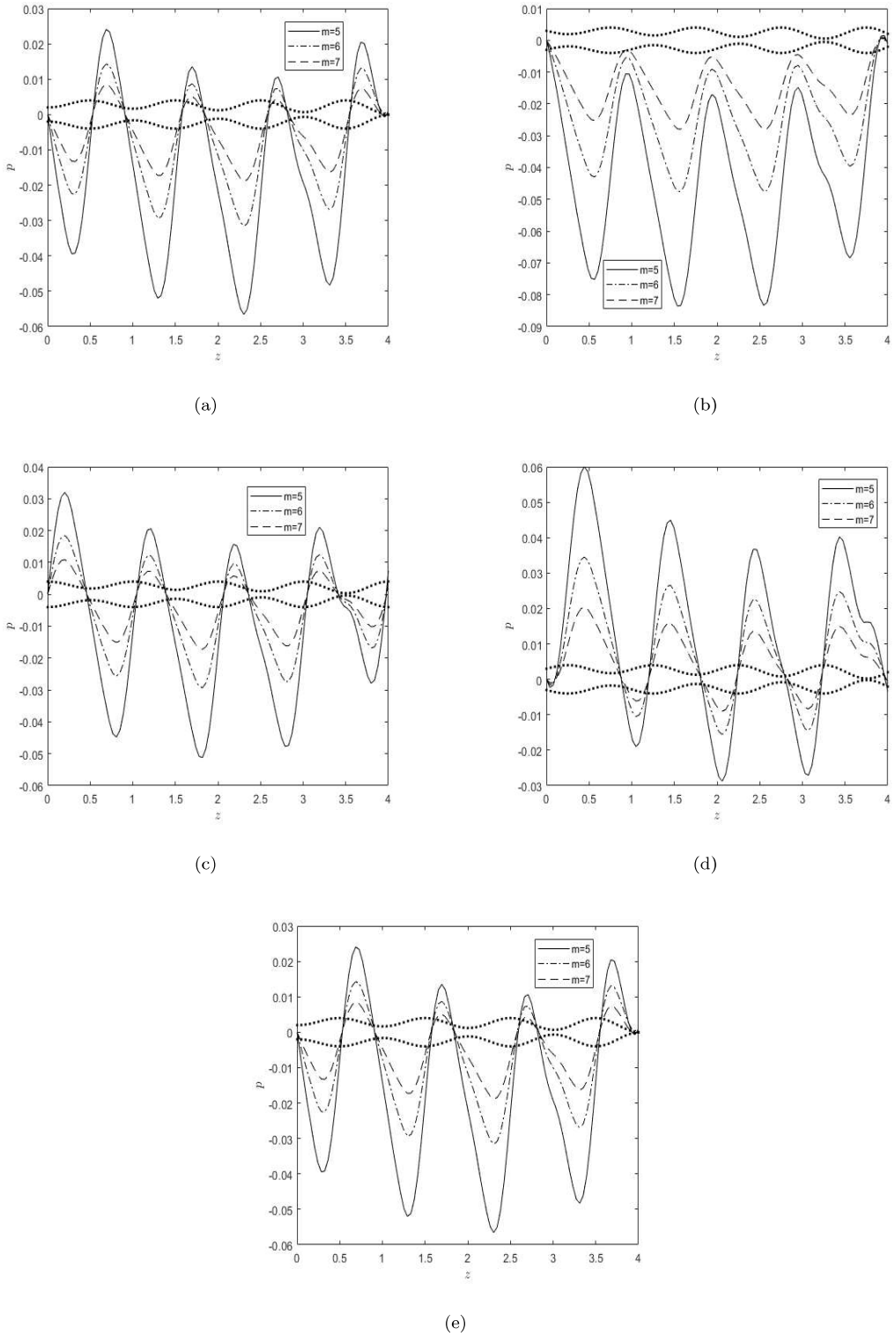

(a) (b)

(c) (d)

(e)

Figure 5.4: The plots show the pressure distribution along the catheterised oesophageal length for $m = 5 - 7$. Other parameters are being fixed as follows: $\phi = 0.49$, $\alpha = 0.4$, $\mu = 0.2$, $\epsilon = 0.1$, $N = 0.1$, $k = 0.07$, (a) $t = 0$, (b) $t = 0.25$, (c) $t = 0.5$, (d) $t = 0.75$, (e) $t = 1$.

In Figures 5.5(a-e), we observe the effects of the coupling number N on the pressure distribution with the introduced catheter. The parameters are set as follows: $\mu = 0.2$, $\phi = 0.49$, $k = 0.07$, $\epsilon = 0.2$, $m = 5$. Here, we observe that the effect of the coupling number is comparatively opposite to that of the micropolar parameter. It is shown that increasing the coupling number $N = 0.2 - 0.4$, i.e., either vortex viscosity increases or the dynamic viscosity decreases, the rise in the magnitude of the curves representing the pressure distribution is greater. Tripathi et al. (2021) got similar results on an asymmetric microchannel without an introduced catheter. Compared to Newtonian fluid, the effort by the oesophageal wall to propel the micropolar fluid is more in the core layer. The reason for this much effort is the increase in the coupling number, i.e., either vortex viscosity increases or the dynamic viscosity decreases its rotation in the micropolar fluid and a catheter inside the oesophagus. It is concluded that in a Newtonian fluid, the pressure decreases Pandey and Pandey (2024b), but due to its microrotation, the presence of fluid particles causes pressure to rise. This led to the conclusion that swallowing a micropolar fluid requires the oesophagus to exert more effort than it normally does. The observation holds for all values of t between 0 and 1.

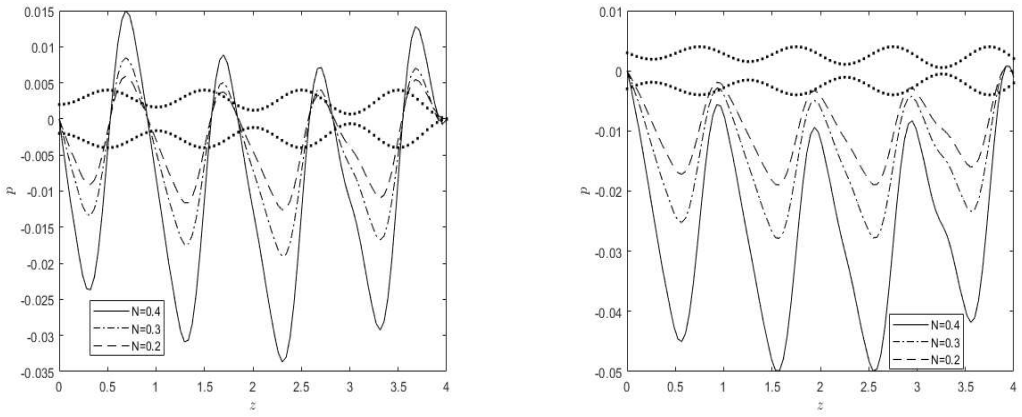

(a) (b)

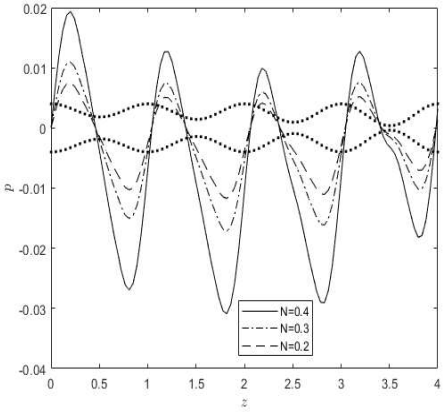

(c)

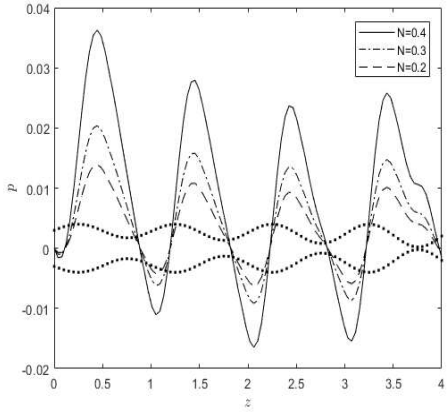

(d)

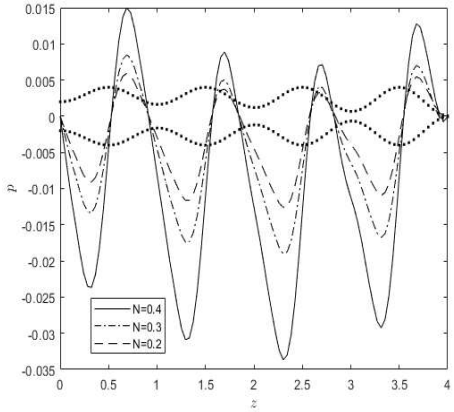

(e)

Figure 5.5: The plots show the pressure distribution along the catheterised oesophageal length for $N = 0.2 - 0.04$. Other parameters are being fixed as follows: $\phi = 0.49$, $\alpha = 0.4$, $\mu = 0.2$, $\epsilon = 0.1$, $m = 5$, $k = 0.07$, (a) $t = 0$, (b) $t = 0.25$, (c) $t = 0.5$, (d) $t = 0.75$, (e) $t = 1$.

The plots in Figures 5.6(a-e) show the pressure difference with the flow rate. These plots have been drawn to get insights by considering micropolar fluid surrounded by Newtonian fluid. Figure (5.6a) shows that the increase in the thickness of the peripheral layer lowers the flow rate. This signifies that the increase in the magnitude of the pressure difference lowers the thickness between the two layers and increases the flow rate. In Figure (5.6b), we observe the effect of introducing a catheter on pressure difference in the oesophageal tube. This effect determines the

enhanced pressure difference in broadening the catheter thickness. This also helps to increase the flow rate of micropolar fluid with fixed micropolar parameter and coupling number. The new dimension of this study is the plots given in Figure 5.6(c-d). Due to the micropolar parameter in the micropolar fluid, the pressure difference decreases when it is increased, i.e., the gyro-viscosity decreases. This result is similar to that of Batool et al. (2024), who did the investigations on exploring microrotational effects and temperature variations in electro-osmotic peristalsis in tapered microchannel and that of Ahmed et al. (2024), who studied the effect of inertial forces on MHD peristaltically driven micropolar fluid through the porous-saturated asymmetric channel using Finite Galerkin approach. The flow rate increases with the rise of the coupling number, i.e., either vortex-viscosity increases or the dynamic viscosity decreases together with the pressure difference. It is concluded that when the bolus starts to propel from the upper oesophageal sphincter, the pressure difference starts lowering with the constituents of the micropolar parameter. In contrast, it starts getting higher with an increased coupling number. This shows that when a patient needs to feed during his examination of swallowing disorder, they can be fed with the fluid having a high micropolar parameter, i.e., the gyro-viscosity increases and low coupling number, i.e., either vortex-viscosity decreases or the dynamic viscosity increases. Lastly, in Figure (5.6e), it is observed that on increasing the dilating amplitude parameter (k), the flow rate reduces and decreases in the magnitude of the pressure difference. This concludes that the pressure difference is required throughout the propulsion of a bolus with the dilating amplitude parameter. Nevertheless, if k becomes zero, we cannot say with certainty that the bolus has taken its part in the stomach for complete further digestion.

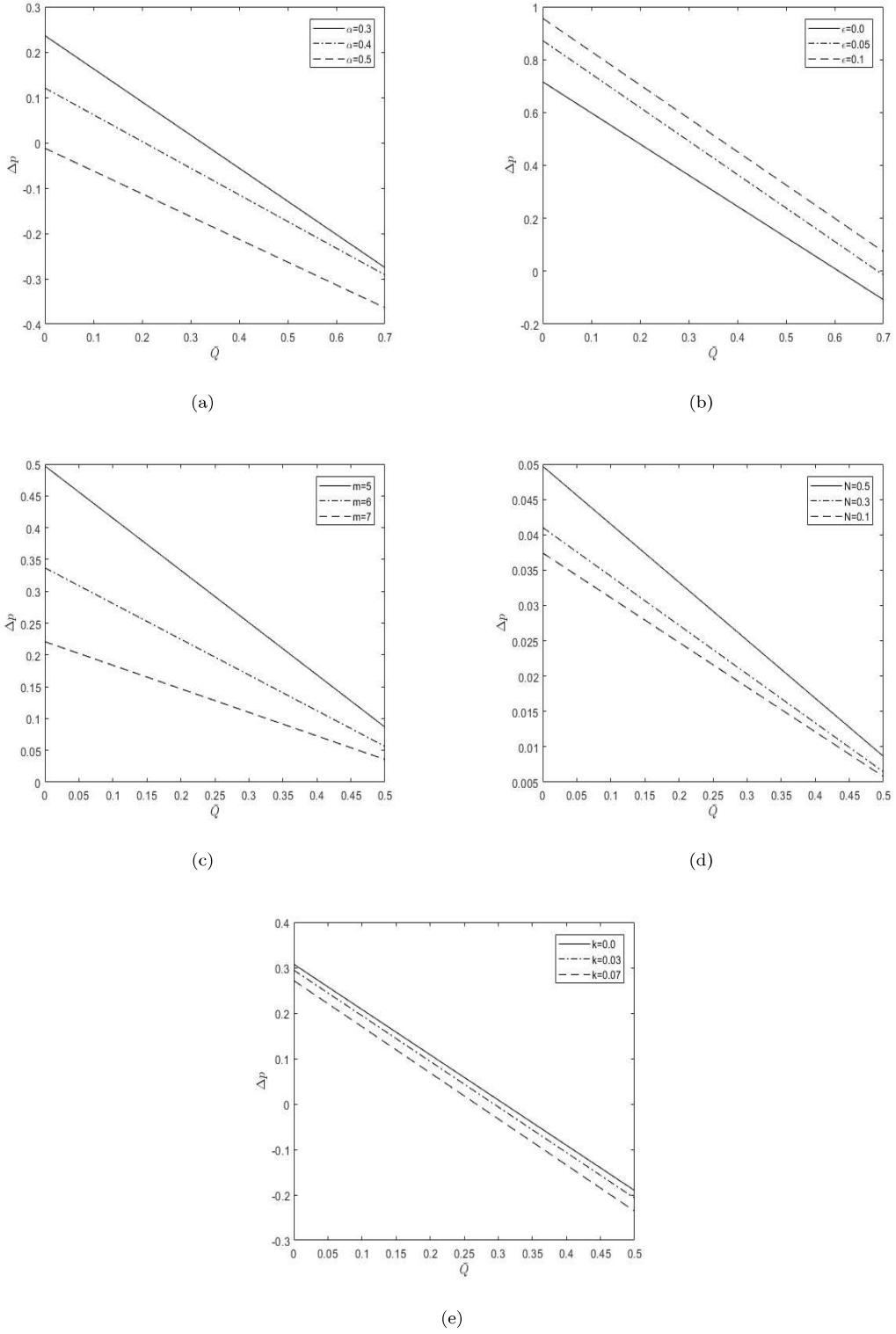

Figure 5.6: The plots show the pressure difference with the time-averaged flow rate for (a) $\alpha = 0.3 - 0.5$, (b) $\epsilon = 0.0 - 0.1$, (c) $m = 5 - 7$, (d) $N = 0.1 - 0.5$, (e) $k = 0.0 - 0.07$, at $t = 0$.

Previously, we observed the effects of the micropolar parameter, i.e., the gyro-viscosity, and the coupling number, i.e., the vortex-viscosity and the dynamic viscosity with a fixed size of the introduced catheter (Figures 5.2, 5.4, 5.5). But now, in the plots of Figures 5.7(a, b), we observe their effects on the magnitude of pressure with the broadening of a catheter thickness. Here, the purpose of choosing the values of catheter thickness (ϵ) is just for illustration. When the micro-polarity in the fluid is lower, it increases the magnitude of pressure, whereas the pressure descends when it gets higher. We noticed that the gap between $m = 5$ and $m = 6$ is more compared to $m = 6$ and $m = 7$. This gap reveals that the sudden spike in the magnitude of pressure enhances the flow rate when the patient is diagnosed with an introduced catheter. The trends are quite similar to the coupling number. However, increasing the coupling effect in the micropolar fluid lowers the complication of a patient with pressure at the same stage. In Figure 5.7c, we observe that increasing the value of the thickness of the catheter keeps the magnitude of pressure higher with the flow rate. This means that broadening the size of a catheter still raises pressure issues until the flow rate lowers.

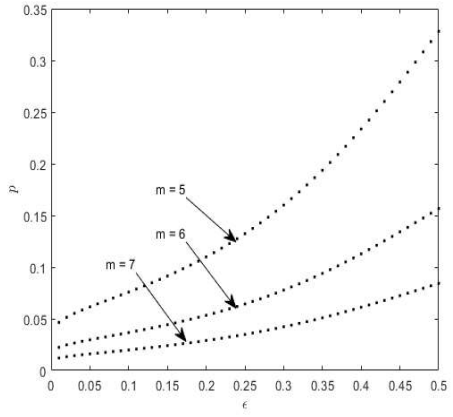

(a)

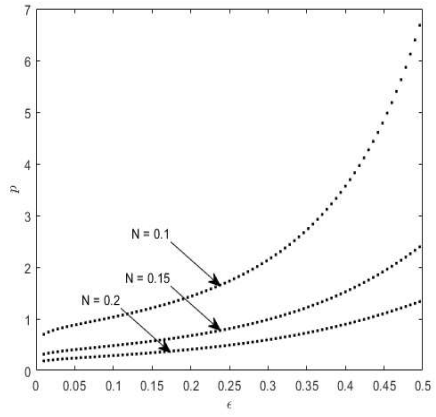

(b)

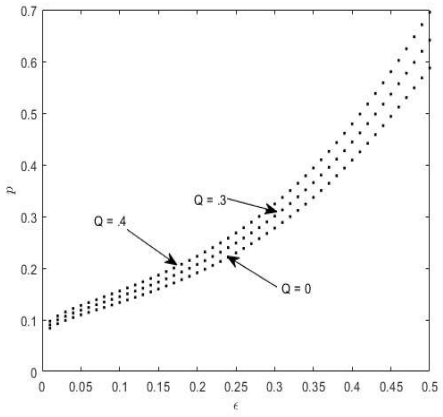

(c)

Figure 5.7: The plots show the rise in the pressure with the broadening of the catheter thickness ϵ for (a) m (micropolar parameter), (b) N (coupling number) and (c) Q (flow rate), at $t = 0$.

One of the most crucial observations regarding the resistance of flow in oesophageal catheterization has been discussed in this analysis. Inserting the catheter into the oesophagus becomes an occlusion resisting the flow. In Figures 5.8(a, b), the impedence increases exponentially on increasing the catheter size corresponding to micropolar parameter values $m = 5,\ 6,\ 7$. This finding agrees with the results obtained in the study of Muthu et al. (2008) and Srinivasacharya and Srikanth (2012) for catheterisation in the artery. A rapidly changing behavior in impedence for $m = 5$ is noted here, increasing slowly. This two-layer model lets us move to the more realistic analysis of impedance investigated here for the micropolar fluid surrounded by Newtonian fluid. The aftermath of coupling number, i.e., vortex-viscosity or the dynamic viscosity on the impedence and the size of the catheter, has been observed, which also helps to increase impedance. Additionally, the impedance increases as catheter size (ϵ) grows. It is observed that a micropolar fluid exhibits more impedance than a Newtonian fluid does.

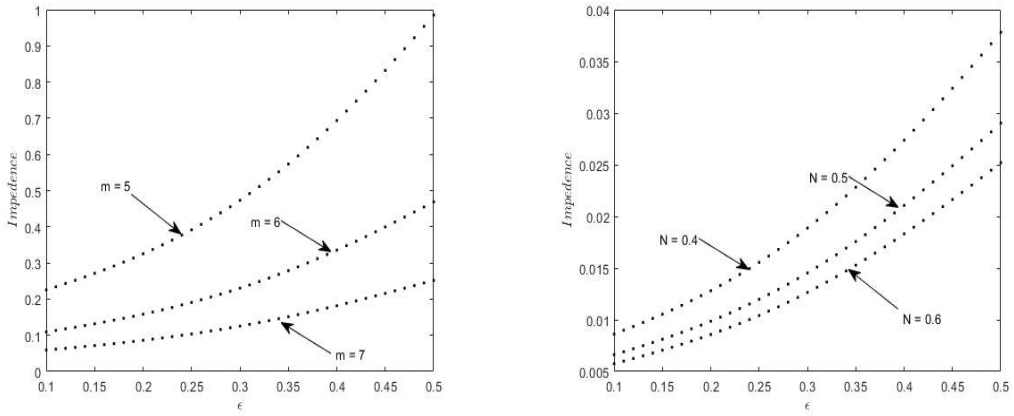

(a) (b)

Figure 5.8: The plots show the resistance to the flow by introduced catheter into the oesophageal lumen that is measured by Impedence with the thickness of catheter for (a) $m = 5 - 7$, and (b) $N = 0.4 - 0.6$.

In Figures 5.9(a, b), we depicted that the increase in flow rate decreases the magnitude of impedence with the decrease in value of the micropolar parameter, i.e., an increase in the gyro-viscosity. It has also been observed that the coupling number, i.e., vortex-viscosity or dynamic viscosity, helps reduce the impedence with the flow rate. It is important to note that, according to prior research on arteries Srivastava and Rastogi (2010) with an introduced catheter, the impedance of the oesophagus increases roughly two to three times during oesophageal catheterization compared to that of the oesophagus without a catheter. As a result, it should be noted that the catheter dramatically affects the physiological characteristics of the flow.

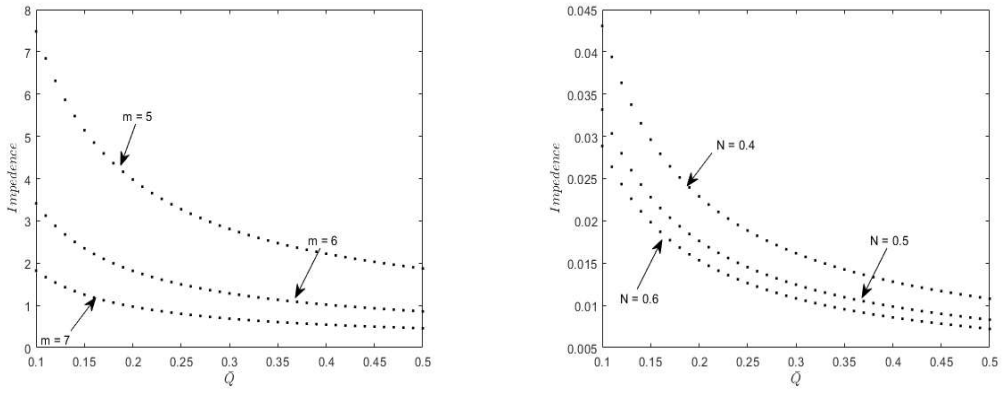

(a) (b)

Figure 5.9: The plots show the resistance to the flow by the introduced catheter into the oesophageal lumen that is measured by Impedence with the time-averaged flow rate for (a) $m = 5 - 7$, and (b) $N = 0.4 - 0.6$.

In Figures 5.10(a-e), we observed the impact of the micropolar parameter, i.e., the gyro-viscosity in the variation of frictional forces due to the catheter wall's surface F_c along the axis of the oesophageal tube. It is observed that increases in the micropolar parameter, i.e., with a decrease in the gyro-viscosity, decrease the frictional force between the introduced catheter and core layer. In contrast, it is less exerting in no catheter case with fixed values of micropolar parameter. This observation continues for various time intervals, i.e., $t = 0$, 0.25, 0.5, 0.75, and 1.

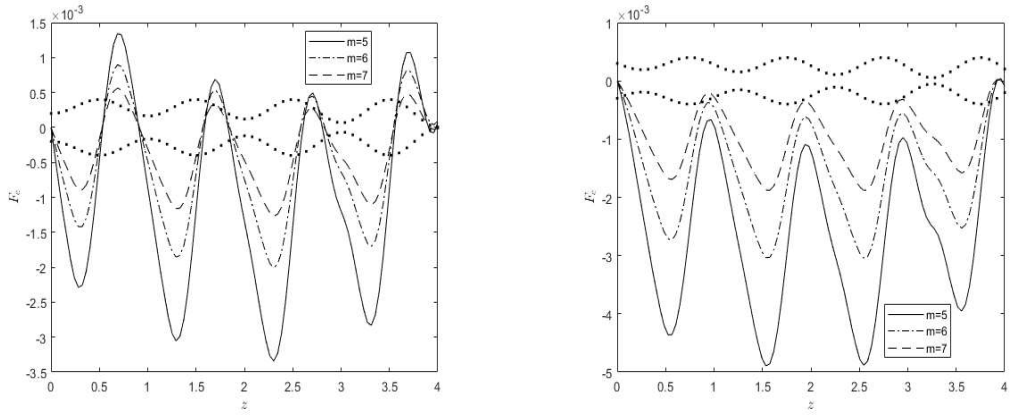

(a) (b)

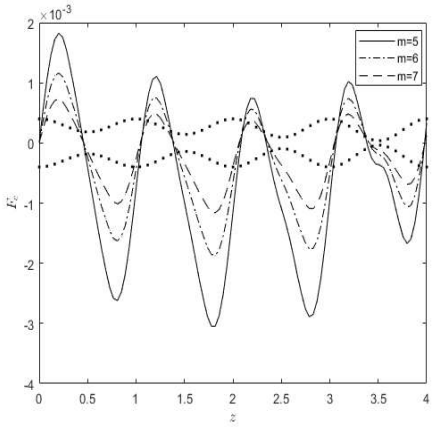

(c)

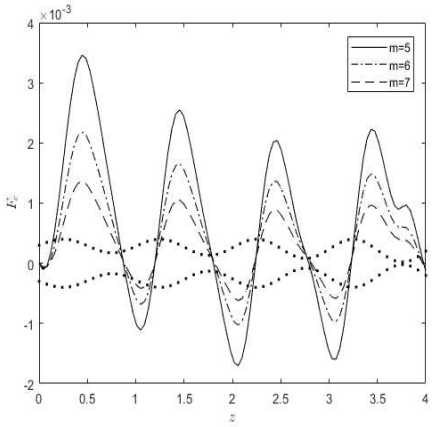

(d)

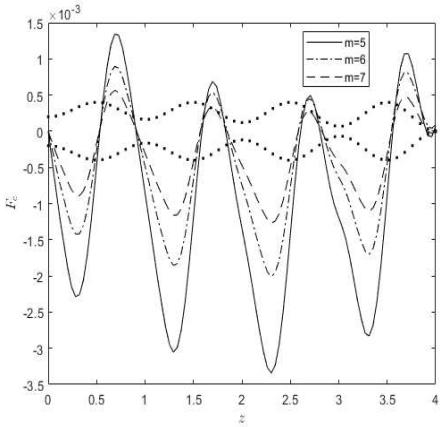

(e)

Figure 5.10: The plots show the effect of the micropolar parameter on the distribution of frictional force along the oesophageal length with the introduced catheter. The parameters are being fixed as follows: $\alpha = 0.4$, $\mu = 0.2$, $\phi = 0.49$, $N = 0.1$ by varying m for (a) $t = 0$ and (b) $t = 0.25$, (c) $t = 0.5$, (d) $t = 0.75$ and (e) $t = 1$.

The plots of Figures 5.11(a-e) show the velocity profile of the core layer that is carried out by micropolar fluid. The catheter is introduced through this layer. The impact of catheterisation reveals that the magnitude of the velocity is getting higher with the broadening of the catheter. As the contraction of the muscles takes place, the rise in the velocity is obtained. It is further observed that as the dilation of the wave amplitude progresses, the spikes in the curves representing velocity magnitude

keep going until the complete drop of the bolus into the stomach. It is concluded from Figures 5.2(a-e) that as the pressure distribution increases throughout the oesophageal length, the velocity increases with the thickness of the catheter.

The increase in the magnitude of velocity can also be seen with the increase in the micropolar parameter, i.e., a decrease in the gyro-viscosity (see Figures 5.12(a-e)). Initially, the magnitude is negative as the head of the bolus enters the oesophagus, but as the bolus progresses, the velocity again shoots up by crossing the zero line, and it is getting maximum for the tail of the next bolus. The cycle continues till the final bolus enters the oesophagus.

In Figures 5.13(a-e), it is observed that the rotational motion of particles in micropolar fluid, influenced by the coupling number, amplifies the velocity magnitude. However, as the coupling number increases, i.e., either an increase in the vortex-viscosity or a decrease in the dynamic viscosity, the velocity initially decreases and eventually becomes negative. Subsequently, it rises again, aiding in the continued propulsion of the bolus toward the lower oesophageal sphincter. The streamlines of the flow are plotted in figure 5.14, which presents the flow pattern in the presence of a catheter.

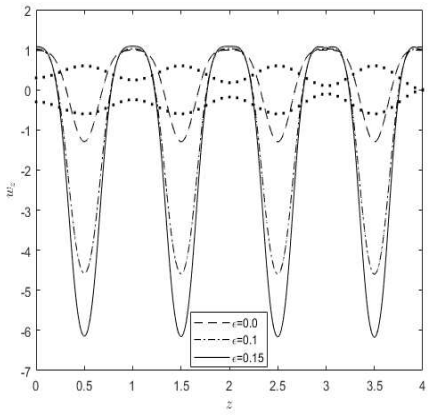

(a)

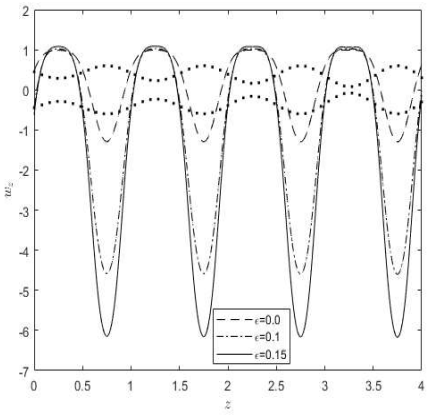

(b)

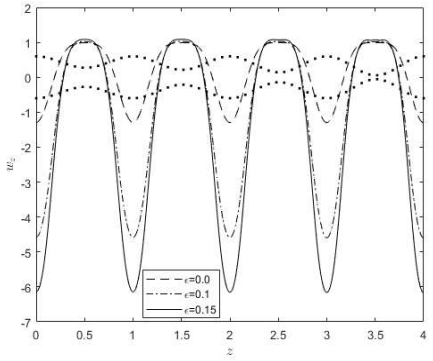

(c)

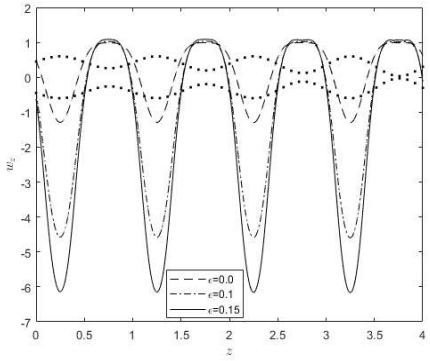

(d)

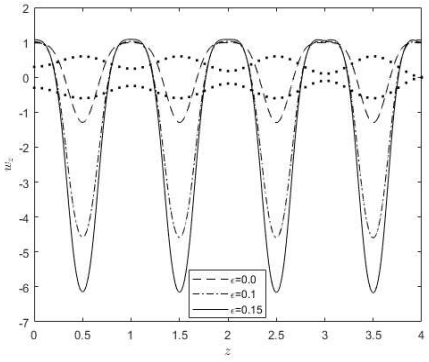

(e)

Figure 5.11: The plots show the effect of the introduced catheter on the velocity profile of the core layer along the oesophageal length for time instants as follows: $t = 0$, (b) $t = 0.25$, (c) $t = 0.5$, (d) $t = 0.75$ and (e) $t = 1$.

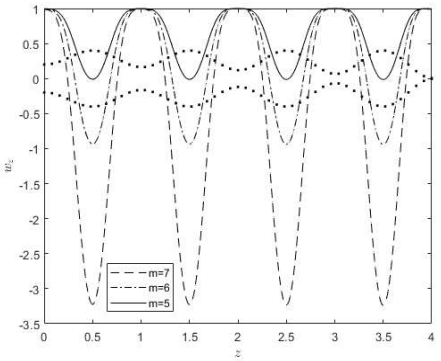

(a)

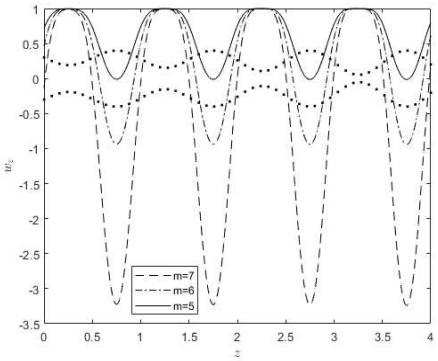

(b)

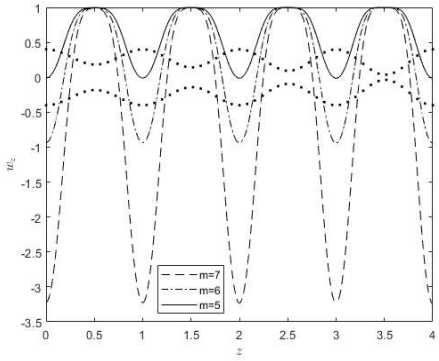

(c)

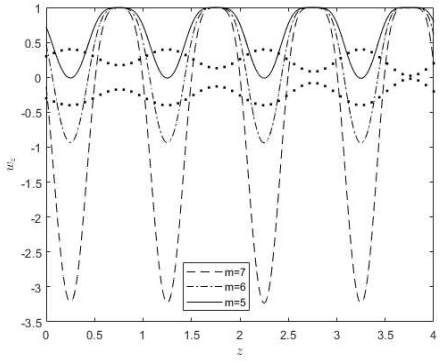

(d)

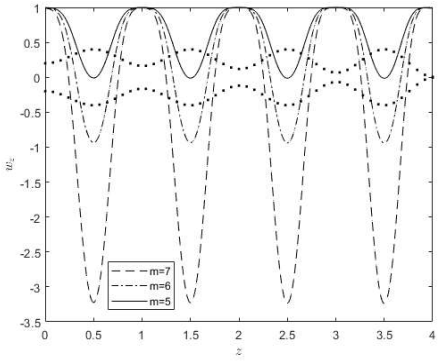

(e)

Figure 5.12: The plots show the effect of the micropolar parameter with the introduced catheter on the velocity profile of the core layer along the oesophageal length for time instants as follows: (a) $t = 0$, (b) $t = 0.25$, (c) $t = 0.5$, (d) $t = 0.75$ and (e) $t = 1$.

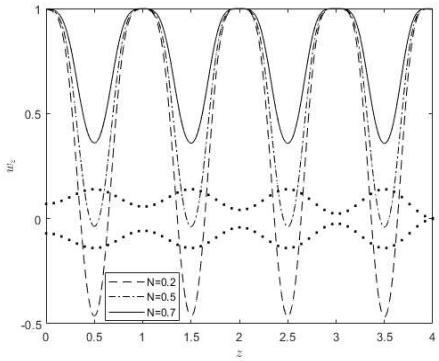

(a)

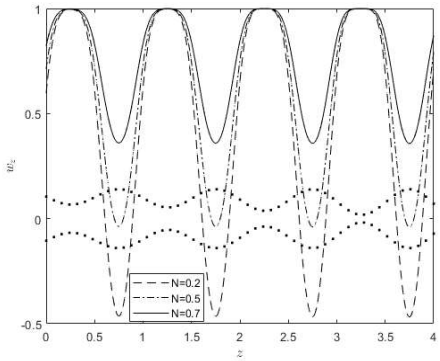

(b)

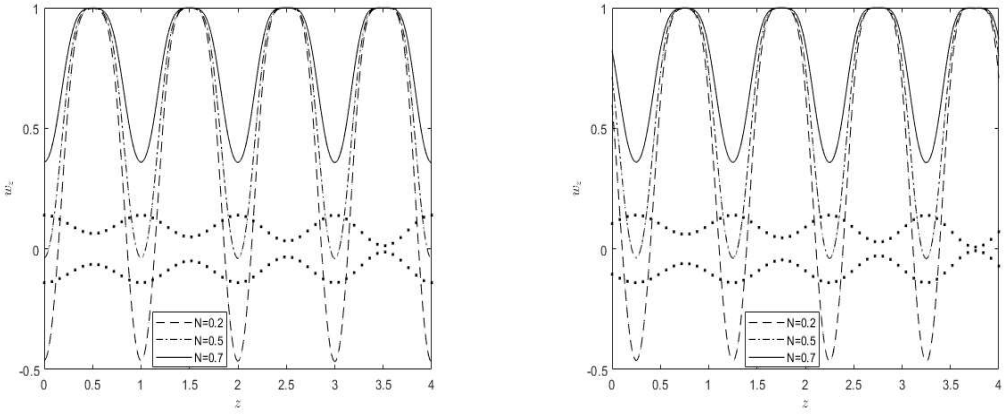

(c) (d)

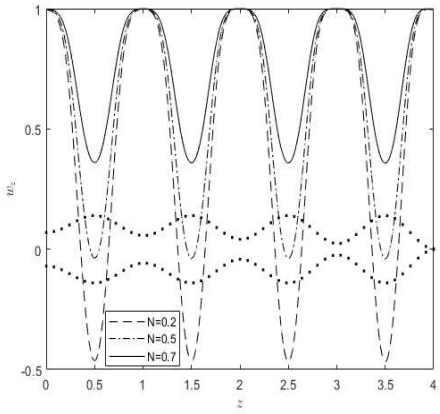

(e)

Figure 5.13: The plots show the effect of the coupling number parameter with the introduced catheter on the velocity profile of the core layer along the oesophageal length for time instants as follows: (a) $t = 0$, (b) $t = 0.25$, (c) $t = 0.5$, (d) $t = 0.75$ and (e) $t = 1$.

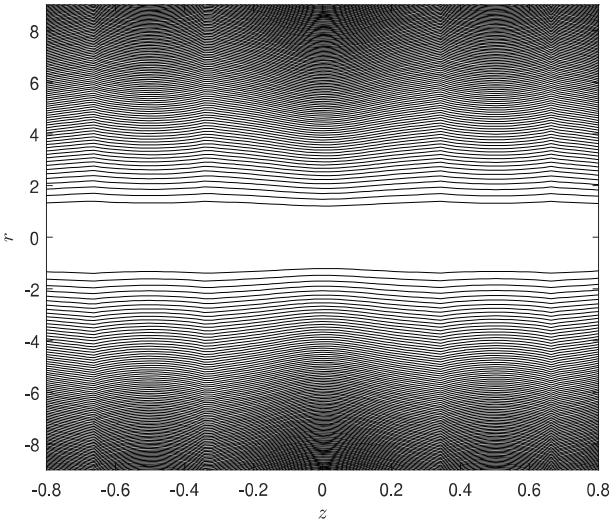

(a)

Figure 5.14: The plot shows the streamline with the introduced catheter in the core layer along the oesophageal length.

5.5 Conclusion

A consistent increase in pressure was observed throughout the oesophagus when a catheter was inserted therein. This is further influenced by the dilating amplitude and micropolar parameters and the coupling number as well. Pressure rises with the coupling number but decreases with the micropolar parameter. We also note an exponential increase in pressure with catheter broadening, particularly when the micropolar parameter diminishes with impedance. Additionally, as pressure increases, the flow rate is enhanced with the dilating amplitude parameter, exacerbating catheter thickness due to impedance further elevating pressure.

In an oesophagus, the presence of a catheter containing micropolar fluid leads to a higher pressure than that with Newtonian fluid. The micropolar parameter and coupling number significantly influence pressure distribution with notable impacts from frictional forces and impedance.

Hence, precaution is necessary when administering feeds with micropolar fluid. Secondary peristalsis during feeding may augment pressure further within the oesophagus, which is already raised by the presence of the catheter.

Key conclusions drawn from the study include:

- Pre-determining the catheter size before insertion to mitigate discomfort and pressure fluctuations caused by both the insertion process and the properties of the micropolar fluid.
- The liquid food or medicine in liquid form should be preferred to be of Newtonian nature.
- Limiting catheter insertion to an optimal point that allows effective feeding without causing undue discomfort or complications.
- Advising against direct oral feeding once a catheter has been inserted through the nasal passage into the oesophagus.

These insights were not previously addressed, making them crucial for pre-diagnosing and managing various swallowing disorders, including achalasia, Barrett's oesophagus, gastroesophageal reflux, sliding hiatus hernia, and others. Such conditions often necessitate pre-diagnostic procedures involving catheter insertion before considering surgical interventions.

Appendix

The governing equations are given as follows:
for peripheral layer:

$$\rho_p\Big(\frac{\partial w_1}{\partial t}+w_1\frac{\partial w_1}{\partial z}+v_p\frac{\partial w_1}{\partial r}\Big)=-\frac{\partial p}{\partial z}+\mu_p\Big(\frac{\partial^2}{\partial r^2}+\frac{1}{r}\frac{\partial}{\partial r}+\frac{\partial^2}{\partial z^2}\Big)w_1, \tag{5.67}$$

$$\rho_p\Big(\frac{\partial v_p}{\partial t}+w_1\frac{\partial v_p}{\partial z}+v_p\frac{\partial v_p}{\partial r}\Big)=-\frac{\partial p}{\partial r}+\mu_p(\frac{\partial^2}{\partial r^2}+\frac{1}{r}\frac{\partial}{\partial r}+\frac{\partial^2}{\partial z^2}-\frac{1}{r^2})v_p, \tag{5.68}$$

$$\frac{1}{r}\frac{\partial}{\partial r}(rv_p)+\frac{\partial}{\partial z}(w_1)=0. \tag{5.69}$$

Note that we replace Laplacian operator ∇^2 with $\frac{\partial^2}{\partial r^2} + \frac{1}{r}\frac{\partial}{\partial r} + \frac{\partial^2}{\partial z^2}$ in the equations (5.67) and (5.68).
for core layer:

$$\rho_c\Big(\frac{\partial w_r}{\partial t} + w_r\frac{\partial w_r}{\partial r} + w_z\frac{\partial w_r}{\partial z}\Big) = -\frac{\partial p}{\partial r} + \Big(\frac{2\mu_c + K}{2}\Big)\Big(\frac{\partial^2 w_r}{\partial r^2} + \frac{1}{r}\frac{\partial w_r}{\partial r} + \frac{\partial^2 w_r}{\partial z^2} - \frac{w_r}{r^2} - K\frac{\partial v_\theta}{\partial z}\Big), \tag{5.70}$$

$$\rho_c\Big(\frac{\partial w_z}{\partial t} + w_r\frac{\partial w_z}{\partial r} + w_z\frac{\partial w_z}{\partial z}\Big) = -\frac{\partial p}{\partial z} + \Big(\frac{2\mu_c + K}{2}\Big)\Big(\frac{\partial^2 w_z}{\partial r^2} + \frac{1}{r}\frac{\partial w_z}{\partial r} + \frac{\partial^2 w_z}{\partial z^2}\Big) + K\Big(\frac{\partial v_\theta}{\partial r} + \frac{v_\theta}{r}\Big), \tag{5.71}$$

$$\rho_c j\Big(\frac{\partial v_\theta}{\partial t} + w_r\frac{\partial v_\theta}{\partial r} + w_z\frac{\partial v_\theta}{\partial z}\Big) = -2Kv_\theta + \Big(\frac{\partial^2 v_\theta}{\partial r^2} + \frac{1}{r}\frac{\partial v_\theta}{\partial r} + \frac{\partial^2 v_\theta}{\partial z^2} - \frac{v_\theta}{r^2}\Big) + K\Big(\frac{\partial w_r}{\partial z} - \frac{\partial w_z}{\partial r}\Big), \tag{5.72}$$

$$\frac{\partial w_r}{\partial r} + \frac{\partial w_z}{\partial z} + \frac{w_r}{r} = 0. \tag{5.73}$$

Note that in our case $G = v_\theta$, so accordingly we replace it in the equations (5.70) - (5.72). The non-dimensional quantities are
$h' = \frac{H}{a}$, $h'_1 = \frac{H_1}{a}$, $r' = \frac{r}{a}$, $z' = \frac{z}{\lambda}$, $w'_1 = \frac{w_1}{c}$, $p' = \frac{pa^2}{c\lambda\mu_c}$, $w'_r = \frac{\lambda w_r}{ac}$, $w'_z = \frac{w_z}{c}$, $v'_\theta = \frac{av_\theta}{c}$, $t' = \frac{ct}{\lambda}$, $j' = \frac{j}{a^2}$, $v'_p = \lambda\frac{v_p}{ac}$, $k' = k\lambda$.

On substituting these non-dimensional quantities in the equations (5.67) to (5.73), we write as follows:
for peripheral layer:

$$\rho_p\Big(\frac{\partial cw'_1}{\partial\frac{\lambda}{c}t'} + cw'_1\frac{\partial cw'_1}{\partial\lambda z'} + \frac{ac}{\lambda}v'_p\frac{\partial cw'_1}{\partial ar'}\Big) = -\frac{\partial\frac{c\lambda\mu_p}{a^2}p'}{\partial\lambda z'} + \mu_c\Big(\frac{\partial^2}{\partial(ar')^2} + \frac{1}{ar'}\frac{\partial}{\partial ar'} + \frac{\partial^2}{\partial(\lambda z')^2}\Big)cw'_1, \tag{5.74}$$

$$\rho_p\Big(\frac{\partial\frac{ac}{\lambda}v'_p}{\partial\frac{\lambda}{c}t'} + cw'_1\frac{\partial\frac{ac}{\lambda}v'_p}{\partial\lambda z'} + \frac{ac}{\lambda}v'_p\frac{\partial\frac{ac}{\lambda}v'_p}{\partial ar'}\Big) = -\frac{\partial\frac{c\lambda\mu_c}{a^2}p'}{\partial ar'} + \mu_p\Big(\frac{\partial^2}{\partial(ar')^2} + \frac{1}{ar'}\frac{\partial}{\partial ar'} + \frac{\partial^2}{\partial(\lambda z')^2} - \frac{1}{(ar')^2}\Big)\frac{ac}{\lambda}v'_p, \tag{5.75}$$

$$\frac{1}{ar'}\frac{\partial}{\partial ar'}(ar'\frac{ac}{\lambda}v'_p) + \frac{\partial}{\partial\lambda z'}(cw'_1) = 0, \tag{5.76}$$

for core layer:

$$\rho_c\Big(\frac{\partial\frac{ac}{\lambda}w_r'}{\partial\frac{\lambda}{c}t'}+\frac{ac}{\lambda}w_r'\frac{\partial\frac{ac}{\lambda}w_r'}{\partial ar'}+cw_z'\frac{\partial\frac{ac}{\lambda}w_r'}{\partial\lambda z'}\Big)=-\frac{\partial\frac{c\lambda\mu_c}{a^2}p'}{\partial ar'}+\Big(\frac{2\mu_c+K}{2}\Big)\Big(\frac{\partial^2\frac{ac}{\lambda}w_r'}{\partial(ar')^2}+\frac{1}{ar'}\frac{\partial\frac{ac}{\lambda}w_r'}{\partial ar'}+\frac{\partial^2\frac{ac}{\lambda}w_r'}{\partial(\lambda z')^2}-\frac{\frac{ac}{\lambda}w_r'}{(ar')^2}-K\frac{\partial\frac{c}{a}v_\theta'}{\partial\lambda z'}\Big),\tag{5.77}$$

$$\rho_c\Big(\frac{\partial cw_z'}{\partial\frac{\lambda}{c}t'}+\frac{ac}{\lambda}w_r'\frac{\partial cw_z'}{\partial ar'}+cw_z'\frac{\partial cw_z'}{\partial\lambda z'}\Big)=-\frac{\partial\frac{c\lambda\mu_c}{a^2}p'}{\partial\lambda z'}+\Big(\frac{2\mu_c+K}{2}\Big)\Big(\frac{\partial^2 cw_z'}{\partial(ar')^2}+\frac{1}{ar'}\frac{\partial cw_z'}{\partial ar'}+\frac{\partial^2 cw_z'}{\partial(\lambda z')^2}\Big)+K\Big(\frac{\partial\frac{c}{a}v_\theta'}{\partial ar'}+\frac{\frac{c}{a}v_\theta'}{ar'}\Big),\tag{5.78}$$

$$\rho_c(a^2j')\Big(\frac{\partial\frac{c}{a}v_\theta'}{\partial\frac{\lambda}{c}t'}+\frac{ac}{\lambda}w_r'\frac{\partial\frac{c}{a}v_\theta'}{\partial ar'}+w_z\frac{\partial\frac{c}{a}v_\theta'}{\partial\lambda z'}\Big)=-2K\frac{c}{a}v_\theta'+\Big(\frac{\partial^2\frac{c}{a}v_\theta'}{\partial(ar')^2}+\frac{1}{ar'}\frac{\partial\frac{c}{a}v_\theta'}{\partial ar'}+\frac{\partial^2\frac{c}{a}v_\theta'}{\partial(\lambda z')^2}-\frac{\frac{c}{a}v_\theta'}{(ar')^2}\Big)+K\Big(\frac{\partial\frac{ac}{\lambda}w_r'}{\partial\lambda z'}-\frac{\partial w_z}{\partial ar'}\Big),\tag{5.79}$$

$$\frac{\partial\frac{ac}{\lambda}w_r'}{\partial ar'}+\frac{\partial cw_z'}{\partial\lambda z'}+\frac{\frac{ac}{\lambda}w_r'}{ar'}=0.\tag{5.80}$$

After dropping the primes ('), the above equations reduce to equations as follows: for peripheral layer $(h_1\le r\le h)$:

$$\delta Re\Big(\frac{\partial w_1}{\partial t}+w_1\frac{\partial w_1}{\partial z}+v_p\frac{\partial w_1}{\partial r}\Big)=-\frac{\partial p}{\partial z}+\mu\Big(\frac{1}{r}\frac{\partial}{\partial r}(r\frac{\partial w_1}{\partial r})+\delta^2\frac{\partial^2 w_1}{\partial z^2}\Big),\tag{5.81}$$

$$\delta^3 Re\Big(\frac{\partial v_p}{\partial t}+w_1\frac{\partial v_p}{\partial z}+v_p\frac{\partial v_p}{\partial r}\Big)=-\frac{\partial p}{\partial r}+\mu\Big(\delta^2\frac{1}{r}\frac{\partial}{\partial r}(r\frac{\partial v_p}{\partial r})+\delta^4\frac{\partial^2 v_p}{\partial z^2}-\delta^2\frac{v_p}{r^2}\Big),\tag{5.82}$$

$$\frac{1}{r}\frac{\partial}{\partial r}(rv_p)+\frac{\partial w_1}{\partial z}=0,\tag{5.83}$$

and for core layer $(\epsilon\le r\le h_1)$:

$$Re\delta^3\Big(w_r\frac{\partial w_r}{\partial r}+w_z\frac{\partial w_r}{\partial z}\Big)=-\frac{\partial p}{\partial r}+\frac{\delta^2}{1-N}\Big(\frac{\partial^2 w_r}{\partial r^2}+\frac{1}{r}\frac{\partial w_r}{\partial r}+\delta^2\frac{\partial^2 w_r}{\partial z^2}-\frac{w_r}{r^2}-N\frac{\partial v_\theta}{\partial z}\Big),\tag{5.84}$$

$$Re\delta\Big(w_r\frac{\partial w_z}{\partial r}+w_z\frac{\partial w_z}{\partial z}\Big)=-\frac{\partial p}{\partial z}+\frac{1}{N-1}\Big(\frac{N}{r}\frac{\partial(rv_\theta)}{\partial r}+\frac{\partial^2 w_z}{\partial r^2}+\frac{1}{r}\frac{\partial w_z}{\partial r}+\delta^2\frac{\partial^2 w_z}{\partial z^2}\Big),\tag{5.85}$$

$$\frac{Re\delta j(1-N)}{N}\Big(w_r\frac{\partial v_\theta}{\partial r}+w_z\frac{\partial v_\theta}{\partial z}\Big)= -2v_\theta+\frac{2-N}{m^2}\Big(\Big(\frac{1}{r}\frac{\partial(rv_\theta)}{\partial r}\Big)+\frac{\partial^2 v_\theta}{\partial z^2}\Big)+\Big(\delta^2\frac{\partial w_r}{\partial z} -\frac{\partial w_z}{\partial r}\Big), \tag{5.86}$$

$$\frac{\partial w_r}{\partial r}+\frac{\partial w_z}{\partial z}+\frac{w_r}{r}=0, \tag{5.87}$$

Note that here $N=\frac{K}{K+\mu_c}$, $m^2=\frac{K(2\mu_c+K)a^2}{\gamma(K+\mu_c)}$, wave number $\delta=\frac{a}{\lambda}$ and Reynolds number $Re=\frac{\rho ac}{\mu_c}$.

Using the approximation of long wavelength and low Reynolds number, i.e., $\delta << 1$, and $Re \to 0$, we can remove the inertial terms and the equations from (5.74) to (5.80) reduces to

$$\frac{\partial p}{\partial z}=\frac{1}{r}\frac{\partial}{\partial r}\Big(r\mu\frac{\partial}{\partial r}\Big)w_1, \tag{5.88}$$

$$\frac{\partial p}{\partial r}=0. \tag{5.89}$$

$$\frac{N}{r}\frac{\partial(rv_\theta)}{\partial r}+\frac{\partial^2 w_z}{\partial r^2}+\frac{1}{r}\frac{\partial w_z}{\partial r}=(1-N)\frac{\partial p}{\partial z}, \tag{5.90}$$

$$2v_\theta+\frac{\partial w_z}{\partial r}-\frac{2-N}{m^2}\frac{\partial}{\partial r}\Big(\frac{1}{r}\frac{\partial}{\partial r}(rv_\theta)\Big)=0, \tag{5.91}$$